

Glucose-driven TOR–FIE–PRC2 signalling controls plant development

<https://doi.org/10.1038/s41586-022-05171-5>

Received: 22 July 2021

Accepted: 1 August 2022

Published online: 14 September 2022

 Check for updates

Ruiqiang Ye^{1,2}✉, Meiyue Wang^{3,4,5}, Hao Du^{1,2}, Shweta Chhajed⁶, Jin Koh⁷, Kun-hsiang Liu^{1,2,8}, Jinwoo Shin^{1,2}, Yue Wu^{1,2}, Lin Shi^{1,2}, Lin Xu³, Sixue Chen^{6,7}, Yijing Zhang^{3,5} & Jen Sheen^{1,2}✉

Nutrients and energy have emerged as central modulators of developmental programmes in plants and animals^{1–3}. The evolutionarily conserved target of rapamycin (TOR) kinase is a master integrator of nutrient and energy signalling that controls growth. Despite its key regulatory roles in translation, proliferation, metabolism and autophagy^{2–5}, little is known about how TOR shapes developmental transitions and differentiation. Here we show that glucose-activated TOR kinase controls genome-wide histone H3 trimethylation at K27 (H3K27me3) in *Arabidopsis thaliana*, which regulates cell fate and development^{6–10}. We identify FERTILIZATION-INDEPENDENT ENDOSPERM (FIE), an indispensable component of Polycomb repressive complex 2 (PRC2), which catalyses H3K27me3 (refs. ^{6–8,10–12}), as a TOR target. Direct phosphorylation by TOR promotes the dynamic translocation of FIE from the cytoplasm to the nucleus. Mutation of the phosphorylation site on FIE abrogates the global H3K27me3 landscape, reprogrammes the transcriptome and disrupts organogenesis in plants. Moreover, glucose–TOR–FIE–PRC2 signalling modulates vernalization-induced floral transition. We propose that this signalling axis serves as a nutritional checkpoint leading to epigenetic silencing of key transcription factor genes that specify stem cell destiny in shoot and root meristems and control leaf, flower and siliques patterning, branching and vegetative-to-reproduction transition. Our findings reveal a fundamental mechanism of nutrient signalling in direct epigenome reprogramming, with broad relevance for the developmental control of multicellular organisms.

Glucose is a universal nutrient and is the main energy supplier, metabolic precursor and source of biomass for most cells. Glucose also functions as an essential regulatory signal that directly or indirectly controls diverse vital processes in multicellular organisms^{1–5}. In photosynthetic plants, CO₂ captured from the atmosphere leads to system-wide glucose signalling that has pivotal roles in multiple developmental processes that are vital to agronomically important traits and crop yield, including germination, stem cell to primordial proliferation, organ size and patterning, as well as shoot branching, flowering and fruit and seed development^{2–5,13–16}. Notably, plant growth hormones and signalling peptides are ineffective in supporting plant development without the glucose signalling networks^{2–4}. However, how glucose signalling modulates cell fates and organogenesis remains largely unknown^{2–5,13–16}. The evolutionarily conserved TOR kinase is a major glucose signalling mediator that integrates nutrients and energy, as well as growth factors, hormones and environmental cues to control growth, development and ageing^{2–5,17–19}. Although plant TOR has been implicated in processes such as meristem activation to shoot and root growth and flowering^{2–5,15,17–22}, the molecular mechanisms remain poorly understood.

Epigenetic regulation on chromatin underlies cell fate specification and developmental transitions, and is a universal mechanism for establishing and maintaining cell and organ identity in plants and animals^{6–10}. PRC2 catalyses histone H3K27me3, triggering epigenetic silencing of key regulatory genes, which are required for cell identity and plasticity to promote differentiation in various developmental programmes^{6–8,10}. Although both PRC2 and TOR are vital for diverse plant developmental processes, no direct molecular connection has been established between the PRC2-mediated global H3K27me3 regulation in organogenesis and the TOR-associated dynamic nutrient and energy signalling network.

Glucose–TOR signalling modulates H3K27me3

To explore new mechanisms of the complex TOR signalling network in plant development, we conducted unbiased chemical screens for various molecular effects of different levels of TOR kinase deficiency in *A. thaliana*^{2–5}. Germinating seeds in liquid nutrient medium were treated with systematically varying concentrations of the potent

¹Department of Molecular Biology and Centre for Computational and Integrative Biology, Massachusetts General Hospital, Boston, MA, USA. ²Department of Genetics, Harvard Medical School, Boston, MA, USA. ³National Key Laboratory of Plant Molecular Genetics, CAS, Centre for Excellence in Molecular Plant Sciences, Shanghai Institute of Plant Physiology and Ecology, Chinese Academy of Sciences, Shanghai, China. ⁴University of the Chinese Academy of Sciences, Beijing, China. ⁵State Key Laboratory of Genetic Engineering, Collaborative Innovation Center of Genetics and Development, Department of Biochemistry, Institute of Plant Biology, School of Life Sciences, Fudan University, Shanghai, China. ⁶Department of Biology, Genetics Institute, Plant Molecular and Cellular Biology Program, University of Florida, Gainesville, FL, USA. ⁷Proteomics and Mass Spectrometry, Interdisciplinary Centre for Biotechnology Research, University of Florida, Gainesville, FL, USA. ⁸State Key Laboratory of Crop Stress Biology for Arid Areas and College of Life Sciences, and Institute of Future Agriculture, Northwest Agriculture and Forestry University, Yangling, China. ✉e-mail: ye@molbio.mgh.harvard.edu; sheen@molbio.mgh.harvard.edu

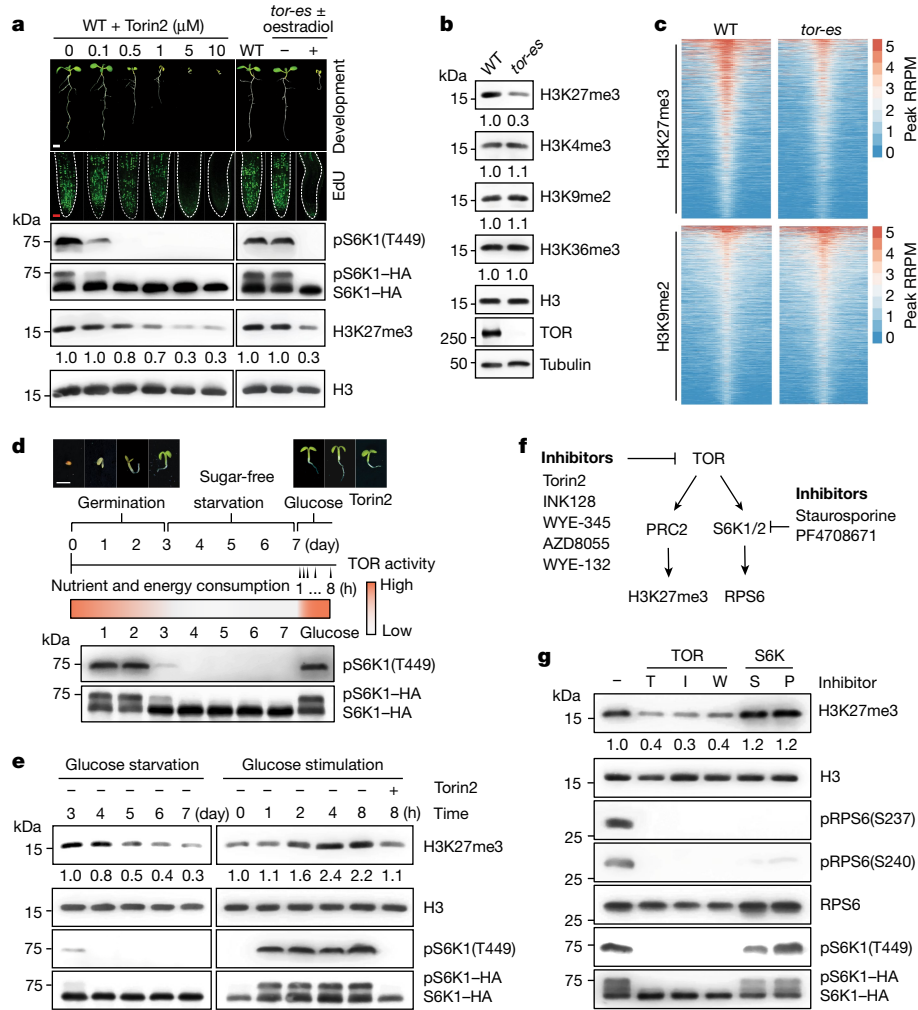


Fig. 1 | Glucose–TOR signalling specifically regulates global H3K27me3 dynamics. **a**, Distinct TOR activity thresholds regulate plant development. Seedling development, EdU staining, pS6K1(T449) phosphorylation and H3K27me3 quantification in WT seedlings treated with different concentrations of Torin2 or in *tor-es* seedlings at 8 days after germination in rich medium. Images are representative of ten seedlings. White scale bar, 2 mm; red scale bar, 25 μ m. **b**, Specific reduction of H3K27me3 levels in 7-day *tor-es* seedlings (10 μ M oestradiol treatment for 3 days). **c**, Heat map of H3K27me3 or H3K9me2 enrichment in WT and *tor-es* seedlings. The colour scale indicates reference-adjusted reads per million (RRPM) surrounding peak summit from the ChIP-Rx-seq data. **d,e**, Glucose–TOR signalling rapidly

regulates H3K27me3 dynamics. **d**, Schematic presentation of experimental design for glucose regulation of TOR activity. **h**, hour. Scale bar, 2 mm. **f,g**, TOR but not S6K regulates global H3K27me3 levels. **g**, S6K activity was monitored by phosphorylation on RPS6 at S237 and S240 (pRPS6(S237) and pRPS6(S240), respectively). Torin2 (T), INK128 (I) and WYE-345 (W) are specific TOR inhibitors; staurosporine (S) and PF-4708671 (P) inhibit S6K1 and S6K2 activity. Values show the relative level of histone modifications compared with the corresponding H3 control relative to the intensity in the WT. Experiments were conducted in three biological repeats with similar results. Samples derive from the same experiment and gels and blots were processed in parallel.

ATP-competitive TOR inhibitor Torin2^{2,4} at the initiation of postembryonic development. S6K phosphorylation, an evolutionarily conserved indicator of TOR activity^{4,21}, was strongly inhibited by Torin2, starting from 0.1 μ M. Higher Torin2 concentrations (5–10 μ M) abolished DNA replication, as indicated by quantitative incorporation of the thymidine analogue 5-ethynyl-2'-deoxyuridine (EdU)⁴ and retarded shoot and root development. Notably, decreased TOR activity resulting from treatment with 0.5–10 μ M Torin2 gradually decreased levels of the epigenomic mark H3K27me3, which is associated with developmental transitions and organ differentiation^{6–10}. This function of TOR signalling in chromatin regulation was validated genetically in mutant plants with oestradiol-inducible RNA-mediated inhibition of TOR expression^{4,21} (*tor-es*), which exhibited suppression of pS6K1(S449), EdU staining, high H3K27me3 and seedling development (Fig. 1a and Extended Data Fig. 1a,b). However, the reduction in H3K27me3 was probably underestimated, partially owing to experimental limitations

when DNA replication was abolished by 5–10 μ M Torin2 or *tor-es*^{4,15} (Fig. 1a).

We next determined the specificity of TOR regulation of chromatin modifications by quantifying major histone methylation marks using immunoblot analyses in seven-day-old wild-type (WT) and *tor-es* *Arabidopsis* seedlings. H3K27me3, but not H3K4me3, H3K9me2 or H3K36me3, was specifically reduced in the *tor-es* mutant (Fig. 1b). We further performed quantitative chromatin immunoprecipitation with an exogenous reference genome followed by deep sequencing²³ (ChIP-Rx-seq). The average density plot and heat map revealed a global reduction of H3K27me3 occupancy in the *tor-es* mutant, whereas the H3K9me2 level was unaffected. The reduction of H3K27me3 in the *tor-es* seedlings was detected throughout the genome (Fig. 1c, Extended Data Fig. 1c,d and Supplementary Table 1), suggesting that the deposition and/or maintenance of H3K27me3 is regulated by TOR.

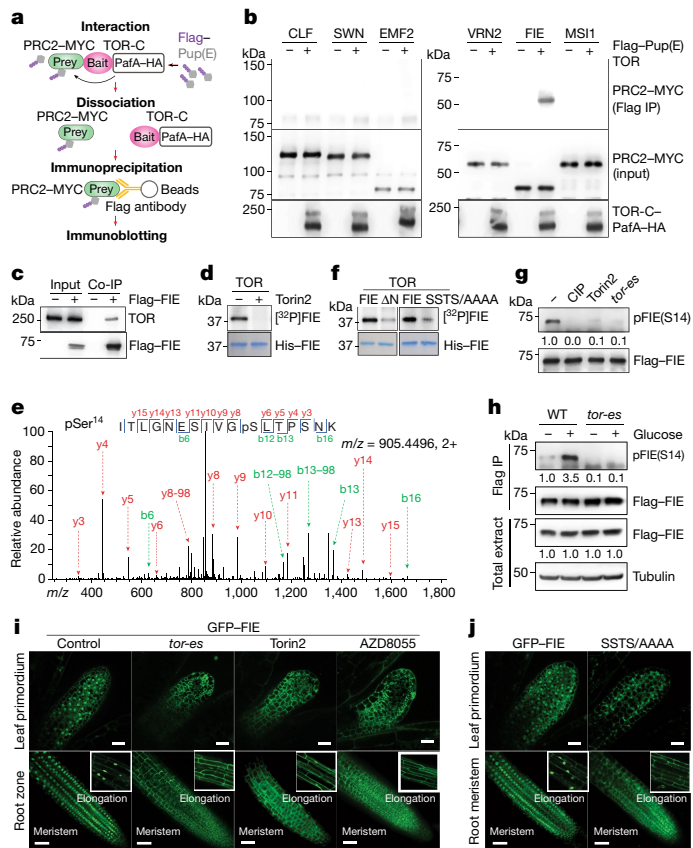


Fig. 2 | Direct TOR phosphorylation promotes translocation of FIE from the cytoplasm to the nucleus. **a**, Schematic of the PUP-IT proximity-tagging system. PafA, a bacterial Pup ligase, is fused to the C terminus (residues 1226–2480) of TOR (TOR-C) (bait). TOR-C-PafA-HA joins 3×Flag-Pup(E) to lysine residues of interacting proteins (prey). The subunits of PRC2 were screened for interaction with TOR-C-PafA-HA by pupylation. **b**, Specific interaction between FIE and TOR. Immunoblot analysis of PUP-IT screening of MYC-tagged PRC2 components with TOR-C-PafA-HA. **c**, TOR interacts with FIE in vivo. Co-immunoprecipitation (Co-IP) of Flag-tagged FIE with TOR from seedlings crosslinked with formaldehyde. Non-transgenic WT seedlings served as the control. **d**, TOR directly phosphorylates FIE in vitro. Top, phosphorylation of His-FIE by immunoprecipitated endogenous TOR is shown by autoradiography. Bottom, Coomassie blue staining, showing protein loading. Torin2 specifically inhibits TOR kinase. **e**, FIE S14 is phosphorylated by TOR in vivo, as shown by tandem mass spectrometry. **f**, Critical TOR phosphorylation sites in FIE. In vitro TOR kinase assays were conducted with FIE and mutants. ΔN , N terminus deletion. SSTS/AAAA, the phosphorylation site mutant. **g**, Detection of FIE phosphorylation in vivo. CIP, calf intestinal alkaline phosphatase. Values are the relative level of phosphorylation over the amount of immunoprecipitated Flag-GFP-FIE (labelled Flag-FIE), with mock treatment set as 1.0. **h**, Glucose enhances pFIE(S14) levels. Immunoblot analysis of pFIE(S14) in immunoprecipitated Flag-GFP-FIE from 7-day starved and 25 mM glucose-stimulated (2 h) WT and *tor-es* plants. **i,j**, Confocal images of GFP-FIE (**i**) and GFP-FIE(SSTS/AAAA) (**j**) in leaf primordia and roots. WT seedlings that were untreated (control) or treated with 10 μ M Torin2 or AZD8055, or *tor-es* seedlings (treated with 10 μ M oestradiol for 3 days). Inset, GFP detected in the root elongation zone. Scale bars, 25 μ m. Images are representative of six seedlings from three biological repeats. Data in **b–g,h** are representative of three biological replicates each. The samples derive from the same experiment and gels and blots were processed in parallel.

We then investigated TOR regulation of H3K27me3 in a physiological context by analysing H3K27me3 dynamics in the well-established heterotrophic to photoautotrophic transition stage when the endogenous sugar derived from the seed reserve is depleted three days after germination. Photosynthesis or exogenous glucose could activate TOR,

which was monitored by the phosphorylation status of pS6K1(T449) under light^{4,15,21} (Fig. 1d,e). *Arabidopsis* seedlings germinated and grown in a sugar-free liquid medium naturally entered a reversible quiescent state in growth and development with decreased TOR activity at 3 to 7 days after germination^{4,15} (Fig. 1d). The H3K27me3 levels were maintained during this period in sugar-containing medium (Extended Data Fig. 1e), but were gradually reduced during the sugar starvation phase, correlating with inactive TOR and stalled seedling development. Glucose addition rapidly stimulated TOR activity and de novo H3K27me3 accumulation within 2 h, suggesting the reprogramming of chromatin states. Consistently, the restoration of H3K27me3 levels was blocked by Torin2 (10 μ M) during glucose stimulation (Fig. 1e).

To ensure TOR kinase specificity and to differentiate TOR regulation of H3K27me3 dynamics from effects of pS6K1(T449) (Fig. 1a), seedlings were treated with structurally distinct chemical inhibitors that target TOR or S6K1 (Fig. 1f). All five of the TOR inhibitors, but not the S6K1 inhibitors^{2,4}, resulted in significant global H3K27me3 reduction. TOR kinase inhibition by Torin2 or AZD8055 led to similar genome-wide reduction of H3K27me3 occupancy as in *tor-es* mutants, as indicated by ChIP-Rx-seq analyses quantified by heat map, average density plot and genome browser view (Fig. 1g and Extended Data Fig. 2a–d and Supplementary Table 2). In seven-day-old glucose-starved seedlings, the conserved components of TOR complex 1 (TORC1), RAPTOR1 (RAP1) and LST8-1 (refs. ^{2–5}), mediated S6K phosphorylation of pRPS6(S237) and pRPS6(S240), which were differentially blocked in the *rap1* and *lst8-1* mutants but not in *rap2* or *lst8-2* mutants^{24–26}. However, *rap1* and *lst8-1* mutants could still substantially restore H3K27me3 levels after 6 h of stimulation with 25 mM glucose (Fig. 1d–g and Extended Data Fig. 2e). These results were consistent with different TOR activity thresholds modulating pS6K1(T449) and H3K27me3 revealed by the chemical inhibitor screens (Fig. 1a,f,g and Extended Data Fig. 2a), and suggest differential TOR kinase activation of distinct substrates beyond the canonical TORC1 (refs. ^{24,25}).

TOR kinase promotes nuclear FIE dynamics

The rapid increase in H3K27me3 stimulated by glucose-TOR signalling and the genome-wide reduction of H3K27me3 in *tor-es* seedlings suggested that TOR might regulate the activity of nuclear PRC2. In postembryonic development, *Arabidopsis* PRC2 comprises four evolutionarily conserved core subunits, including a methyltransferase (CURLY LEAF (CLF) or SWINGER (SWN)), a scaffold protein (EMBRYONIC FLOWER2 (EMF2) or VERNALIZATION2 (VRN2)), the histone-binding protein MULTICOPY-SUPPRESSOR-OF-IRA1 (MSI1) and FIE, which contains a WD40 structural fold^{6–8,10–12} (Extended Data Fig. 3a). We first examined the transcript and protein levels of PRC2 core components in *tor-es* or Torin2-treated seedlings; only CLF transcript and EMF2 protein were partially reduced (Extended Data Fig. 3b,c). We postulated that TOR might interact with and phosphorylate the core components and activate PRC2. We used pupylation-based interaction tagging²⁷ (PUP-IT), a proximity-tagging system, to identify candidate substrates of TOR. We generated a haemagglutinin-tagged protein fusion of the bacterial Pup ligase (PafA) and the C-terminal kinase domain of TOR (TOR-C-PafA-HA) and co-expressed this with Flag-tagged Pup(E) and MYC-tagged PRC2 components in mesophyll protoplasts (Fig. 2a). FIE was specifically pupylated by TOR-C-PafA-HA (Fig. 2b). FIE is an essential and unique component of PRC2 complex, as the *fie* null mutant abolishes global H3K27me3 and limits organogenesis beyond germination¹². The specific interaction between TOR and FIE in vivo was confirmed by co-immunoprecipitation, which was significantly enhanced after 2 h of stimulation with 5–50 mM glucose (Fig. 2c and Extended Data Fig. 4a). FIE was directly phosphorylated in vitro by the TOR kinase immunoprecipitated from *Arabidopsis* plants⁴; the phosphorylation reaction was specifically and completely inhibited by Torin2 (Fig. 2d).

To identify the TOR phosphorylation site in FIE, we analysed phosphorylation sites from *in vitro* TOR kinase assays by liquid chromatography–tandem mass spectrometry (LC–MS/MS). We identified four main phosphorylation sites within the N-terminal domain of FIE: S10, S14, T16 and S18 (Extended Data Fig. 4b–f). Structural modelling of FIE based on embryonic ectoderm development protein (EED), the human orthologue of FIE, identified the flexible and serine- and threonine-rich N-terminal domain as a potential target for phosphorylation^{11,28} (Extended Data Fig. 4g). The phosphorylation of pS14, pT16 and pS18 in endogenous FIE was validated by LC–MS/MS analyses in glucose-stimulated seedlings (Fig. 2e and Extended Data Fig. 4b). Since S14A was the only single mutation in FIE that exhibited significantly reduced phosphorylation in the TOR kinase assay, the other phosphorylation sites probably have partially redundant and cooperative functions (Extended Data Fig. 4h). The N-terminal 34-residue deletion (Δ N) or the quadruple phosphorylation site mutant (SSTS to AAAA) of FIE was barely phosphorylated by TOR (Fig. 2f and Extended Data Fig. 4h). The key phosphorylation sites in FIE proteins are largely conserved among diverse flowering plants, including *Arabidopsis*, *Brassica*, soybean, rice, maize and wheat, and possibly in fly (ESC) and human (EED) orthologues of plant FIE²⁹ (Extended Data Fig. 5a,b).

To functionally validate and quantify endogenous FIE phosphorylation, we generated a phosphopeptide-specific antibody targeting the phosphorylated form of FIE at S14, which was the most highly enriched and confident site validated by LC–MS/MS analyses *in vitro* and *in planta* (Fig. 2e and Extended Data Fig. 4b,d). This antibody specifically recognized the TOR-phosphorylated FIE, but not the S14A mutant (Extended Data Fig. 5c). Immunoprecipitation from seedlings did not detect *in vivo* phosphorylation of FIE at S14 (pFIE(S14)) following treatment with calf intestine phosphatase. Moreover, pFIE(S14) was largely abolished in seedlings treated with Torin2 or in *tor-es* plants (Fig. 2g). Immunoblot analysis showed that after starvation, pFIE(S14) was significantly induced within 2 h by 5–50 mM glucose; this effect was abolished in 7-day-old *tor-es* seedlings (Fig. 2h and Extended Data Fig. 5d). These results demonstrated that the N terminus of FIE is directly phosphorylated in glucose-TOR signalling.

We next explored how TOR phosphorylation regulates FIE function. Immunoblot analysis showed that the stability of GFP–FIE was not affected in *tor-es* or Torin2-treated plants (Extended Data Fig. 5e). Complexes formed by recombinant *Arabidopsis* PRC2 with the wild-type or the phosphorylation-site SSTS/AAAA mutant of FIE exhibited similar H3K27me3 methyltransferase activity *in vitro* (Extended Data Fig. 5f). Cytoplasmic FIE–GFP has been reported to interact exclusively with MEDEA (MEA) methyltransferase and not with CLF or SWN in inflorescences. It was postulated that the cytoplasmic FIE–GFP might have non-nuclear functions beyond chromatin methylation³⁰. We tested the possibility that TOR phosphorylation promotes the cytoplasm-to-nucleus translocation of GFP–FIE to activate PRC2 (Extended Data Fig. 6a). Distinct from the predominant nuclear localization in control plants grown in sugar-containing nutrient medium, GFP–FIE was detected primarily in the cytoplasm in differentiating leaf primordia and root elongation and meristem zones in *tor-es* plants or following treatment of 5-day seedlings with Torin2 or AZD8055 (Fig. 2i and Extended Data Fig. 6b). However, the nuclear localization of other PRC2 components in roots—GFP–CLF, SWN–GFP, EMF2–GFP and MSI1–GFP—was not altered by Torin2 treatment (Extended Data Fig. 6c). Notably, the mutation of four TOR-phosphorylated sites (SSTS/AAAA) compromised the nuclear translocation of GFP–FIE in protoplasts and in transgenic plants without affecting the protein level (Fig. 2j) and Extended Data Fig. 6b,d,e. The ratio of cytoplasmic to nuclear GFP–FIE (C:N ratio) increased quantitatively in the root elongation zone during the sugar starvation phase and decreased rapidly upon glucose treatment after five days of starvation (Extended Data Fig. 6f–j). Time-lapse live imaging showed that glucose rapidly stimulated real-time nuclear translocation of GFP–FIE within 2–4 h, coinciding with the increase in

H3K27me3 level (Fig. 1e and Supplementary Video). In contrast to the conventional view of a preformed nuclear PRC2 with FIE as a key static component interacting with CLF or SWN and binding to H3K27me3 in the nucleus^{6–8,10–12,30}, our findings revealed that FIE serves as a molecular bridge, directly linking glucose-TOR signalling with PRC2-regulated H3K27me3 dynamics and gene silencing.

TOR phosphorylation of FIE controls development

To elucidate the molecular functions of the phosphorylated FIE by TOR kinase, we introduced GFP–FIE with or without the phosphorylation site mutation SSTS/AAAA, under the control of the *FIE* promoter, into heterozygous *fie*/*+* plants. Homozygous *GFP-FIE/fie* and *SSTS/AAAA/fie* plants were selected for genome-wide H3K27me3 and transcriptome analyses. Conditional *fie* mutants that bypass embryonic lethality were also generated to provide a parallel comparison with *SSTS/AAAA/fie* (Extended Data Fig. 7a–d). The oestradiol-inducible *fie-amiR-es* transgenic lines eliminated FIE protein and exhibited consistent aberrant small, narrow and curled true leaves sharing some features with the occasional *FIE* co-suppressed plants³¹ (Extended Data Fig. 7b–d). The *fie* null mutant seeds generated with the heterozygous *fie*/*+cdka;1*/*+* pollen forms only undifferentiated callus-like structures after germination and blocks further postembryonic development¹². The *SSTS/AAAA/fie* and *fie-amiR-es* mutants had a weaker effect and remained capable of postembryonic development and organogenesis powered by photosynthesis or exogenous glucose⁴, thus providing a valuable platform to investigate the physiological functions of the glucose-TOR–FIE–PRC2 signalling network.

Quantitative immunoblot and ChIP-Rx–seq analyses revealed markedly decreased global H3K27me3 levels across the genome in the 14-day vegetative shoots of *SSTS/AAAA/fie* and *fie-amiR-es* mutants compared with those in WT and *GFP-FIE/fie* plants (Fig. 3a,b, Extended Data Fig. 7e,f and Supplementary Table 3). The *SSTS/AAAA/fie* mutant showed a larger reduction in H3K27me3 than those resulting from TOR inhibition, suggesting that the phosphorylation mutant of FIE was decoupled from other TOR-regulated processes, including DNA replication that could limit H3K27me3 dilution when PRC2 was inhibited^{2–5,15} (Fig. 1a and Extended Data Figs. 1b–d and 2b–d). As a parallel control, GFP–FIE expression in the *fie* null mutant restored the H3K27me3 landscape (Fig. 3a,b, Extended Data Fig. 7e,f and Supplementary Table 3). Genome-wide H3K27me3 target genes previously identified by ChIP analyses in 14-day to 20-day WT seedlings significantly overlapped with our data from quantitative ChIP-Rx–seq analyses in 14-day WT shoots^{12,32} (Extended Data Fig. 7g). Consistent with the genome-wide profiling, H3K27me3 occupancy was decreased at selected target loci with key developmental roles^{6–8,12,31,32} in the *SSTS/AAAA/fie* and *fie-amiR-es* mutants (Fig. 3c).

Transcriptome profiling by RNA-seq identified a total of 3,969 genes ($|\log_2 \text{fold change}| \geq 1; q \leq 0.05, n = 3$) that were dysregulated in the 14-day shoots of *SSTS/AAAA/fie* and *fie-amiR-es* plants (Fig. 3d and Supplementary Table 4). To uncover the biological functions of the TOR–FIE–PRC2 signalling network, we defined the putative direct target genes that were marked by H3K27me3 and upregulated in the *SSTS/AAAA/fie* mutant (Extended Data Fig. 8a and Supplementary Table 5). Gene ontology analysis of 1,081 ($\log_2 \text{fold change} \geq 1; q \leq 0.05$) TOR–FIE–PRC2 target genes revealed a notable enrichment for transcription factors and regulators controlling a broad spectrum of developmental programmes (Extended Data Fig. 8b and Supplementary Table 6). We identified 192 transcription factor genes (Supplementary Table 7), including master regulators with essential roles in stem cell identity, cell fate determination, patterning and developmental transitions, that were significantly upregulated and associated with reduction of H3K27me3 in *SSTS/AAAA/fie* and *fie-amiR-es* mutants (Fig. 3e and Supplementary Tables 5 and 7). In particular, the expression of shoot apical meristem (SAM)-specific transcription factors defining the

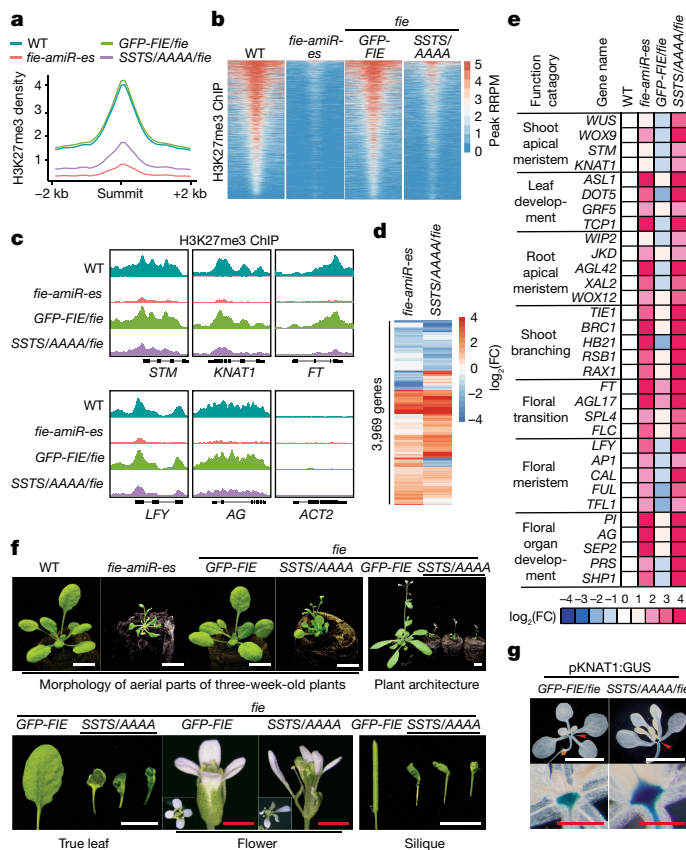


Fig. 3 | The targeted FIE phosphorylation mutation alters the global H3K27me3 landscape to reprogramme the transcriptome and disrupt organogenesis. **a**, Reduction of global H3K27me3 levels in 14-day-old *fie* mutant plants. Metaplots show ChIP-Rx-seq read density of H3K27me3 \pm 2 kb from their peak summits. Chromatin immunoprecipitation with sequencing (ChIP-seq) data are normalized with an exogenous reference genome. **b**, Depletion of H3K27me3 in *fie* mutants. Heat map of H3K27me3 enrichment. The colour scale indicates RRPM surrounding the peak summit, obtained from the ChIP-Rx-seq data. **c**, The IGV browser view of H3K27me3 occupancy at PRC2 target genes. *ACT2*, a non-PRC2-target gene, serves as a negative control. **d**, Transcriptome reprogramming in 14-day *fie* mutants. The heat map shows transcriptomic changes of *fie-amiR-es* (versus WT) and *SSTS/AAAA* (versus *GFP-FIE*) from RNA-seq analyses. FC, fold change. **e**, Comparative expression analyses of key transcription factor genes in diverse developmental programmes. Heat map of RNA-seq data from triplicate biological samples prepared from WT, *fie-amiR-es*, *GFP-FIE* and *SSTS/AAAA/fie* plants. The RNA expression data were normalized to the value in WT plants. **f**, The *fie* mutants display broad developmental aberrations. The *fie-amiR-es* and *SSTS/AAAA/fie* mutants exhibit small, narrow and curled leaves and flower prematurely at 21 days. The *SSTS/AAAA/fie* mutants develop thin, short and terminal inflorescence with aborted flower buds, narrow, split and twisted sepals and petals, and enlarged carpel, as well as short, bulged and contorted siliques (at 30 days). **g**, GUS reporter detection in 14-day-old *GFP-FIE/fie* and *SSTS/AAAA/fie* mutant plants transfected with pKNAT1:GUS. Arrowheads indicate SAM. Three biological replicates, $n > 10$ plants per experiment. White scale bar, 10 mm; red scale bar, 1 mm.

indeterminant cell fate³³ increased in the mutant plants. The abnormal expression of root quiescent centre and stem cell regulators^{34,35} were detected in the 14-day shoots. The key floral integrators controlling vegetative-to-reproductive transition were precociously derepressed at the vegetative seedling stage. We also observed the ectopic activation of floral meristem and floral homeotic genes³⁶ in seedlings. Important transcription factor genes governing leaf development^{37,38} as well as shoot branching^{16,39} were also overexpressed in the *SSTS/AAAA/fie* and *fie-amiR-es* mutants (Fig. 3e, Extended Data Fig. 8c and Supplementary Tables 5 and 7).

In 7-day seedlings grown in liquid medium and optimal for starvation and glucose, and in *tor-es* experiments^{4,15,21}, quantitative PCR with reverse transcription (RT-qPCR) analysis showed that a subset of TOR–FIE–PRC2–H3K27me3 target genes were upregulated, and this was correlated with a reduction of H3K27me3, as shown by chromatin immunoprecipitation with quantitative PCR (ChIP–qPCR) analysis (Extended Data Fig. 8d,e). Consistently, in the sugar-starved 7-day seedlings, glucose initiated the repression of these genes, which was correlated with elevated H3K27me3 at 6 h (Extended Data Fig. 8f,g). Although target gene regulation by *tor-es* or glucose was more subtle in 7-day seedlings than in 14-day *SSTS/AAAA/fie* and *fie-amiR-es* mutant plants (Fig. 3e and Extended Data Fig. 8c), our findings suggest that the glucose–TOR–FIE–PRC2 signalling pathway controls target genes encoding key transcription factors via an epigenomic mechanism (Supplementary Table 7). Further research will be required to elucidate the detailed integration of distinct TOR signalling mechanisms in spatiotemporal modulation of epigenomic and transcriptomic controls of key regulators in diverse processes during different stages of postembryonic development at organ, tissue and single-cell levels.

The consequences of H3K27me3 and transcriptome reprogramming in *SSTS/AAAA/fie* plants were clearly manifested in the profound disruption of temporal and spatial orders of the innate genetic programmes guiding plant differentiation and development^{31,33–40}. Of note, in 21- to 24-day-old plants covering broader developmental stages, the *SSTS/AAAA/fie* mutants displayed grossly aberrant developmental phenotypes, similar to those in *fie-amiR-es* lines, including early flowering, abnormalities in the size, morphology and patterning of leaves, flowers and siliques, reduced branching with miniature plant architecture and terminal flowers and infertility (Fig. 3f and Extended Data Fig. 7d), as well as enlarged SAM indicated by the *pKNAT1:GUS* reporter (Fig. 3g). The expression of *GFP-FIE* in the null *fie* mutant fully restored the size and morphology of organs, whole plant architecture, developmental timing and fertility (Fig. 3f and Extended Data Fig. 7d). These data indicate that TOR phosphorylation of FIE has a vital role in gating PRC2-mediated epigenetic reprogramming in diverse postembryonic developmental programmes throughout the plant life.

Glucose–TOR–FIE signalling gates vernalization

To further explore how this direct molecular link between glucose–TOR signalling and H3K27me3 dynamics is involved in a defined developmental programme, we studied vernalization-induced flowering. This process involves H3K27me3-mediated silencing of the floral transcription repressor gene *FLOWERING LOCUS C* (*FLC*) by prolonged cold treatment, which provides a paradigm to study environmentally regulated epigenetic dynamics during developmental phase transitions^{40–43}. *FLC* was activated in the *SSTS/AAAA/fie* and *fie-amiR-es* mutants (Fig. 3e), and sugar accumulation was found to be associated with prolonged cold treatment and floral induction^{13,44,45}, but its physiological importance remains unknown. To decipher the role of glucose–TOR signalling in vernalization-mediated floral transition, we showed that prolonged cold exposure significantly induced sustained glucose accumulation in the Col-*FRIGIDA* (*FRI*) line (Fig. 4a). The functional *FRI* allele confers the vernalization-dependent floral transition in *Arabidopsis*⁴². The elevation of endogenous TOR activity quantified by pS6K1(T449) closely matched the profile of intrinsic glucose surge during vernalization in *FRI* and was abolished by potent and specific TOR inhibitors, Torin2 or INK128 (1 μ M) (Figs. 1f,g and 4b). These results suggest that glucose-induced TOR activation may regulate vernalization.

To strengthen the molecular link between the glucose–TOR–FIE–PRC2 signalling relay and vernalization, we quantified *FLC* expression, PRC2-mediated H3K27me3 marks on the *FLC* chromatin and flowering time. *FRI* was introduced into *tor-es*, *GFP-FIE/fie* and *SSTS/AAAA/fie* mutants for comparative analyses. Cold-induced repression of *FLC* was

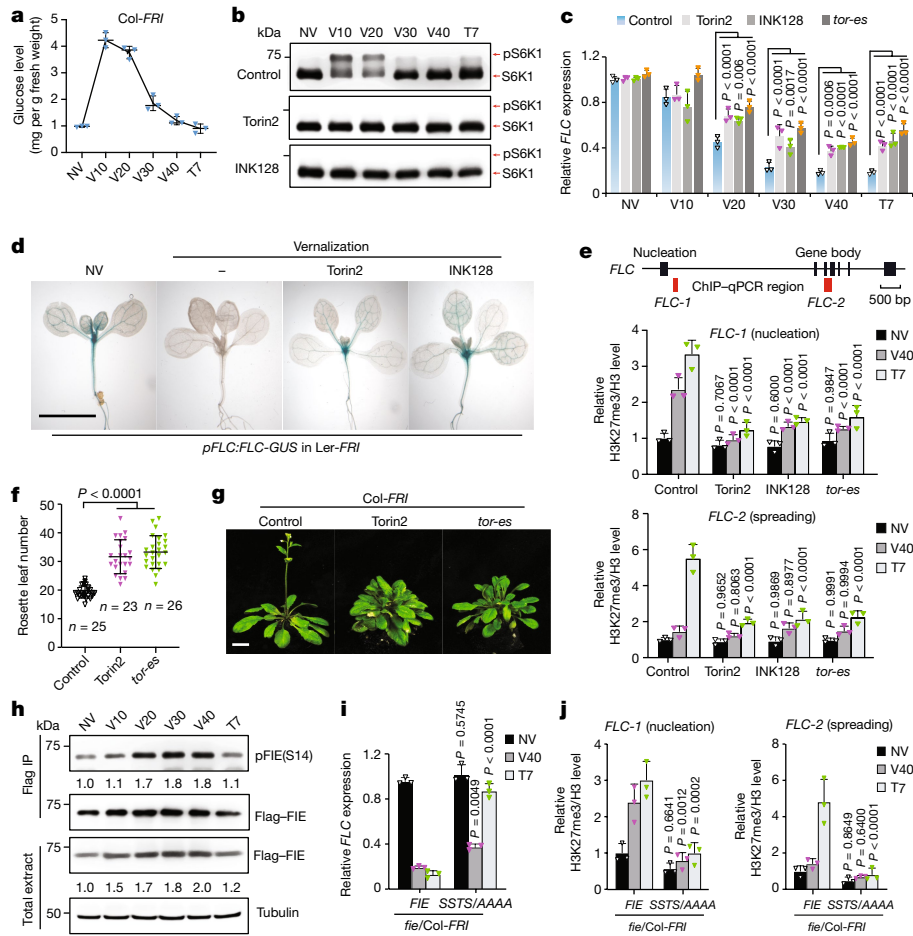


Fig. 4 | Glucose–TOR–FIE signalling stimulates vernalization-mediated floral transition. **a**, Vernalization induces glucose accumulation in *Col-FRI* plants. NV, non-vernalized; V, vernalization days at 4 °C; T, post-cold days at 22 °C. $n = 3$ biological repeats. **b**, Vernalization stimulates TOR activity. TOR activity was indicated by the band shift of S6K1-HA, indicating S6K1 phosphorylation (pS6K1). **c**, TOR promotes *FLC* repression by vernalization. **d**, TOR inhibitors prevent vernalization-mediated repression of the *FLC* reporter. Histochemical staining of the *pFLC:FLC-GUS* (*Ler-FRI*) transgenic plant before and after vernalization without or with TOR inhibitors (1 μM Torin2 or INK128). Scale bar, 10 mm. **e**, TOR deficiency reduces H3K27me3 levels at *FLC*. Black boxes indicate exons and red boxes show regions selected for H3K27me3 ChIP-qPCR analyses. bp, base pairs. *FLC-1* and *FLC-2* are located in the nucleation and spreading regions of H3K27me3 at *FLC*, respectively. **f**, TOR is required for vernalization. Flowering time was analysed by counting rosette leaf numbers when bolting after vernalization. Data are mean ± s.d. n is the number of individual plants. **g**, Representative flowering phenotype of the

indicated plant at bolting after vernalization. Scale bar, 10 mm. **h**, FIE phosphorylation increases during vernalization. Immunoblot analysis of total and phosphorylated FIE proteins after vernalization treatment. Values show the relative level of phosphorylated FIE over total immunoprecipitated Flag-FIE. The non-vernalized level is set as 1.0. **i**, Repression of *FLC* by vernalization is diminished in *SST5/AAA*/*fie/Col-FRI* plants. **j**, Vernalization-induced H3K27me3 levels are compromised at *FLC* during two silencing phases. **c,i**, Relative expression of *FLC* versus *UBC21* was normalized to the non-vernalized level in control or *fie/Col-FRI* plants. **e,j**, Relative H3K27me3 versus H3 level was normalized to that of control or *fie/Col-FRI* plants under the non-vernalized condition. Data in **c,e,i,j** are mean ± s.d. from 3 biological replicates; two-way ANOVA with Tukey's multiple comparisons test. **f**, One-way ANOVA with Tukey's multiple comparisons test. Data in **b,h** are representative of three biological replicates each. The samples derive from the same experiment and gels and blots were processed in parallel.

impaired by specific TOR inhibitors and in the *tor-es* mutant (Fig. 4c), whereas the activation of *VERNALIZATION INSENSITIVE3* (*VIN3*) was unaffected during the same cold exposure (Extended Data Fig. 9a). To monitor the *FLC* expression dynamics and locations in intact plants, the transgenic *pFLC:FLC-GUS* (*Ler-FRI*) line carrying the *FLC* promoter and a *GUS* translational fusion was visualized by histochemical staining. Consistent with the RNA expression results, the reduction of *FLC* reporter expression in the SAM and vasculature upon vernalization was prevented by TOR inhibitors (Fig. 4d).

Cold-induced silencing of *FLC* by PRC2 was characterized by two phases: the initial nucleation and the propagation of H3K27me3 on the *FLC* locus⁴². We found that both phases were impaired in *tor-es* or by TOR inhibitors (Fig. 4e and Extended Data Fig. 9b). In addition, plants with conditional TOR deficiency during vernalization exhibited delayed flowering time after returning to ambient temperature with full TOR

activity (Fig. 4f,g). These results demonstrate that *FLC* repression during vernalization requires TOR activity. Prolonged cold treatment markedly increased the accumulation of glucose (Fig. 4a), pS6K1 (Fig. 4b), pFIE(S14), total FIE protein level (Fig. 4h) and the quantitative nuclear localization of GFP–FIE (Extended Data Fig. 9c,d), which prompted the initial nucleation of H3K27me3 (refs. ^{4,40,42,43}). The phosphorylation and nuclear localization of FIE were sustained even after the large glucose surge declined after 30 days of vernalization, presumably owing to continuous energy expenditure with limited photosynthesis under cold treatment^{4,46}. The steady-state glucose level and TOR activity, and FIE phosphorylation and localization resumed to support normal and dynamic photosynthesis-driven glucose–TOR–FIE signalling for the maintenance and spreading of H3K27me3 after plants were returned to warm temperature^{4,40,42,43,46}. The differential dynamics of pS6K1 and pFIE dephosphorylation during vernalization (Fig. 4b,h) suggested

that distinct glucose–TOR substrates for divergent downstream signalling processes may exhibit different kinetics and regulation. Vernalization-mediated *FLC* repression was diminished during the cold exposure but recovered after cold in the *SSTS/AAAA/fie* mutant (Fig. 4i), resembling the vernalization-defective *vin3*, *vrn2* and *vrn5* mutants^{40,42}. Consistently, the nucleation and spreading of H3K27me3 enrichment at *FLC* in response to vernalization were abolished in the *SSTS/AAAA/fie* mutant plants (Fig. 4j and Extended Data Fig. 9e). Together, these data indicate that specific FIE phosphorylation by glucose–TOR signalling modulates vernalization-mediated floral transition.

Discussion

Here we report a direct molecular link between glucose–TOR signalling and PRC2 regulation. TOR kinase, activated by glucose derived from local or systemic carbon sources, phosphorylates FIE at S14 and other cooperative sites (S10, T16 and S18) and promotes its translocation from the cytoplasm to the nucleus to enhance PRC2 activity. In the nucleus, the active FIE–PRC2 complex is probably recruited by transcription repressors, *cis*-regulatory elements and non-coding RNAs to deposit H3K27me3 for silencing of key transcription factor genes that modulate cell fate determination, developmental transitions and organ patterning in *Arabidopsis*^{6,8,10,40,42,43,47–49}. We propose that this signalling axis serves as a nutritional checkpoint for regulating PRC2 activity throughout key differentiation phases and processes during plant postembryonic development (Figs. 3 and 4 and Extended Data Fig. 10). Notably, there is a recent report of TOR regulation of H3K27me3 target genes that are activated by stress conditions beyond normal developmental programmes or vernalization⁵⁰.

A notable feature of the postembryonic growth and development in plants is the indeterminate stem cell niche in the meristems, which continuously supply new cells for root, leaf, stem, flower and fruit organogenesis beyond the simple embryo designed for nutrient storage and dormancy^{12,33,34}. Our genome-wide analyses define diverse master transcription factors as target genes of the glucose–TOR–PRC2 signalling network and key to major developmental programmes (Figs. 3 and 4, Extended Data Figs. 8 and 10 and Supplementary Table 7). This glucose-stimulated epigenomic network promotes faithful differentiation and developmental transitions, including stem cell to meristem or primordium switch, juvenile to adult organogenesis, axillary meristem to branching, and reproductive processes from flowering to silique development (Extended Data Fig. 10a). This molecular switch ensures that the proliferation and differentiation processes during organ growth and patterning in time and space are integrated and coordinated with adequate nutrient and energy support. Crucially, under the prolonged cold condition, the glucose-activated TOR–FIE–PRC2 relay overrides the default vegetative programme by silencing the floral repressor *FLC*, which may suggest how sugars support the vernalization-induced flowering⁴⁴ (Extended Data Fig. 10b). These molecular connections provide a long-sought mechanistic explanation for how glucose signalling regulates multiple developmental processes in plants. This study advances a conceptual understanding of how multicellular organisms transmit systemic nutrient information to remodel global chromatin states and modulate local cellular chromatin regulators, thus orchestrating the transcriptional landscape that is central to cell fate regulation in diverse developmental programmes.

Online content

Any methods, additional references, Nature Research reporting summaries, source data, extended data, supplementary information, acknowledgements, peer review information; details of author contributions and competing interests; and statements of data and code availability are available at <https://doi.org/10.1038/s41586-022-05171-5>.

- Krejci, A. & Tennesen, J. M. Metabolism in time and space—exploring the frontier of developmental biology. *Development* **144**, 3193–3198 (2017).
- Shi, L., Wu, Y. & Sheen, J. TOR signaling in plants: conservation and innovation. *Development* **145**, dev160887 (2018).
- Li, L., Liu, K. H. & Sheen, J. Dynamic nutrient signaling networks in plants. *Annu. Rev. Cell Dev. Biol.* **37**, 341–367 (2021).
- Xiong, Y. et al. Glucose–TOR signalling reprograms the transcriptome and activates meristems. *Nature* **496**, 181–186 (2013).
- Dobrelon, T. et al. TOR signaling and nutrient sensing. *Annu. Rev. Plant Biol.* **67**, 261–285 (2016).
- Mozgova, I. & Hennig, L. The polycomb group protein regulatory network. *Annu. Rev. Plant Biol.* **66**, 269–296 (2015).
- Pu, L. & Sung, Z. R. PcG and trxG in plants—friends or foes. *Trends Genet.* **31**, 252–262 (2015).
- Bieluszewski, T., Xiao, J., Yang, Y. & Wagner, D. PRC2 activity, recruitment, and silencing: a comparative perspective. *Trends Plant Sci.* **26**, 1186–1198 (2021).
- Atlasi, Y. & Stunnenberg, H. G. The interplay of epigenetic marks during stem cell differentiation and development. *Nat. Rev. Genet.* **18**, 643–658 (2017).
- Schuettengruber, B., Bourbon, H. M., Di Croce, L. & Cavalli, G. Genome regulation by polycomb and trithorax: 70 years and counting. *Cell* **171**, 34–57 (2017).
- Margueron, R. et al. Role of the polycomb protein EED in the propagation of repressive histone marks. *Nature* **461**, 762–767 (2009).
- Bouyer, D. et al. Polycomb repressive complex 2 controls the embryo-to-seedling phase transition. *PLoS Genet.* **7**, e1002014 (2011).
- Bernier, G. & Perilleux, C. A physiological overview of the genetics of flowering time control. *Plant Biotechnol. J.* **3**, 3–16 (2005).
- Yu, S., Lian, H. & Wang, J. W. Plant developmental transitions: the role of microRNAs and sugars. *Curr. Opin. Plant Biol.* **27**, 1–7 (2015).
- Li, X. et al. Differential TOR activation and cell proliferation in *Arabidopsis* root and shoot apices. *Proc. Natl. Acad. Sci. USA* **114**, 2765–2770 (2017).
- Barbier, F. F., Dun, E. A., Kerr, S. C., Chabikwa, T. G. & Beveridge, C. A. An update on the signals controlling shoot branching. *Trends Plant Sci.* **24**, 220–236 (2019).
- Deprost, D. et al. The *Arabidopsis* TOR kinase links plant growth, yield, stress resistance and mRNA translation. *EMBO Rep.* **8**, 864–870 (2007).
- Ryabova, L. A., Robaglia, C. & Meyer, C. Target of Rapamycin kinase: central regulatory hub for plant growth and metabolism. *J. Exp. Bot.* **70**, 2211–2216 (2019).
- Wu, Y. et al. Integration of nutrient, energy, light, and hormone signalling via TOR in plants. *J. Exp. Bot.* **70**, 2227–2238 (2019).
- Ren, M. et al. Target of rapamycin signaling regulates metabolism, growth, and life span in *Arabidopsis*. *Plant Cell* **24**, 4850–4874 (2012).
- Xiong, Y. & Sheen, J. Rapamycin and glucose-target of rapamycin (TOR) protein signaling in plants. *J. Biol. Chem.* **287**, 2836–2842 (2012).
- Caldana, C. et al. Systemic analysis of inducible target of rapamycin mutants reveal a general metabolic switch controlling growth in *Arabidopsis thaliana*. *Plant J.* **73**, 897–909 (2013).
- Orlando, D. A. et al. Quantitative ChIP-seq normalization reveals global modulation of the epigenome. *Cell Rep.* **9**, 1163–1170 (2014).
- Anderson, G. H., Veit, B. & Hanson, M. R. The *Arabidopsis* AtRaptor genes are essential for post-embryonic plant growth. *BMC Biol.* **3**, 12 (2005).
- Moreau, M. et al. Mutations in the *Arabidopsis* homolog of LST8/GbetaL, a partner of the target of Rapamycin kinase, impair plant growth, flowering, and metabolic adaptation to long days. *Plant Cell* **24**, 463–481 (2012).
- Forzani, C. et al. Mutations of the AtYAK1 kinase suppress TOR deficiency in *Arabidopsis*. *Cell Rep.* **27**, 3696–3708.e3695 (2019).
- Liu, Q. et al. A proximity-tagging system to identify membrane protein-protein interactions. *Nat. Methods* **15**, 715–722 (2018).
- Kallberg, M. et al. Template-based protein structure modeling using the RaptorX web server. *Nat. Protoc.* **7**, 1511–1522 (2012).
- Tie, F., Siebold, A. P. & Harte, P. J. The N-terminus of *Drosophila* ESC mediates its phosphorylation and dimerization. *Biochem. Biophys. Res. Commun.* **332**, 622–632 (2005).
- Oliva, M. et al. FIE, a nuclear PRC2 protein, forms cytoplasmic complexes in *Arabidopsis thaliana*. *J. Exp. Bot.* **67**, 6111–6123 (2016).
- Katz, A., Oliva, M., Mosquna, A., Hakim, O. & Ohad, N. FIE and CURLY LEAF polycomb proteins interact in the regulation of homeobox gene expression during sporophyte development. *Plant J.* **37**, 707–719 (2004).
- Zhang, X. et al. Whole-genome analysis of histone H3 lysine 27 trimethylation in *Arabidopsis*. *PLoS Biol.* **5**, e129 (2007).
- Aichinger, E., Kornet, N., Friedrich, T. & Laux, T. Plant stem cell niches. *Annu. Rev. Plant Biol.* **63**, 615–636 (2012).
- Pierre-Jerome, E., Drapé, C. & Benfey, P. N. Regulation of division and differentiation of plant stem cells. *Annu. Rev. Cell Dev. Biol.* **34**, 289–310 (2018).
- Denyer, T. et al. Spatiotemporal developmental trajectories in the *Arabidopsis* root revealed using high-throughput single-cell RNA sequencing. *Dev. Cell* **48**, 840–852.e845 (2019).
- Liu, C., Thong, Z. & Yu, H. Coming into bloom: the specification of floral meristems. *Development* **136**, 3379–3391 (2009).
- Wang, L. et al. Transcriptional regulation of strigolactone signalling in *Arabidopsis*. *Nature* **583**, 277–281 (2020).
- Petricka, J. J., Clay, N. K. & Nelson, T. M. Vein patterning screens and the defectively organized tributaries mutants in *Arabidopsis thaliana*. *Plant J.* **56**, 251–263 (2008).
- Yang, Y. et al. The TIE1 transcriptional repressor controls shoot branching by directly repressing BRANCHED1 in *Arabidopsis*. *PLoS Genet.* **14**, e1007296 (2018).
- Menon, G., Schulten, A., Dean, C. & Howard, M. Digital paradigm for Polycomb epigenetic switching and memory. *Curr. Opin. Plant Biol.* **61**, 102012 (2021).
- Ruelens, P. et al. FLOWERING LOCUS C in monocots and the tandem origin of angiosperm-specific MADS-box genes. *Nat. Commun.* **4**, 2280 (2013).

42. Yang, H. et al. Distinct phases of Polycomb silencing to hold epigenetic memory of cold in *Arabidopsis*. *Science* **357**, 1142–1145 (2017).
43. Questa, J. I., Song, J., Geraldo, N., An, H. & Dean, C. *Arabidopsis* transcriptional repressor VAL1 triggers Polycomb silencing at FLC during vernalization. *Science* **353**, 485–488 (2016).
44. Purvis, O. N. Vernalization of fragments of embryo tissue. *Nature* **145**, 462 (1940).
45. Klotke, J. K., Gatzke, J. & Heyer, N. A.G. Impact of soluble sugar concentrations on the acquisition of freezing tolerance in accessions of *Arabidopsis thaliana* with contrasting cold adaptation—evidence for a role of raffinose in cold acclimation. *Plant Cell Environ.* **27**, 1395–1404 (2004).
46. Zhao, Y., Antoniou-Kourounioti, R. L., Calder, G., Dean, C. & Howard, M. Temperature-dependent growth contributes to long-term cold sensing. *Nature* **583**, 825–829 (2020).
47. Heo, J. B. & Sung, S. Vernalization-mediated epigenetic silencing by a long intronic noncoding RNA. *Science* **331**, 76–79 (2011).
48. Xiao, J. et al. Cis and trans determinants of epigenetic silencing by Polycomb repressive complex 2 in *Arabidopsis*. *Nat. Genet.* **49**, 1546–1552 (2017).
49. Zhou, Y. et al. Telobox motifs recruit CLF/SWN-PRC2 for H3K27me3 deposition via TRB factors in *Arabidopsis*. *Nat. Genet.* **50**, 638–644 (2018).
50. Dong, Y. et al. TOR represses stress responses through global regulation of H3K27 trimethylation in plants. Preprint at *bioRxiv* <https://doi.org/10.1101/2021.03.28.437410> (2021).

Publisher's note Springer Nature remains neutral with regard to jurisdictional claims in published maps and institutional affiliations.

Springer Nature or its licensor holds exclusive rights to this article under a publishing agreement with the author(s) or other rightsholder(s); author self-archiving of the accepted manuscript version of this article is solely governed by the terms of such publishing agreement and applicable law.

© The Author(s), under exclusive licence to Springer Nature Limited 2022

Methods

Plasmid constructs and the generation of transgenic plants

The pFIE:Flag-GFP-FIE construct includes 2.5 kb upstream and 1.3 kb downstream sequences of the *FIE* coding region in the pCAMBIA1300 binary vector as previously described for generating transgenic plants⁵¹. The triple Flag-tag sequence was introduced along with the promoter sequence and *GFP* was inserted between the Flag sequence and the first ATG codon sequences. The phosphorylation site mutation pFIE-Flag-GFP-FIE (SSTS/AAAA) construct was generated by replacing the *FIE* sequence using site-directed mutagenesis. These binary plasmids were transformed into heterozygote *fie*^{+/−} (GK-534F01-020364) mutant plants by using the *Agrobacterium tumefaciens* (strain GV3101)-mediated floral-dip method⁵². Positive transformants were selected based on hygromycin resistance and confirmed by immunoblot analysis using an anti-Flag antibody. At the T3 generation, *GFP-FIE/fie* and *SSTS/AAAA/fie* plants were confirmed by genotyping using primers listed in Supplementary Table 8.

To generate the oestradiol-inducible *FIE* artificial miRNA mutant (*fie-amiR-es*) transgenic plants, optimal *amiRNAs* were first selected using the epitope-tagged protein-based *amiRNA* (ETPamir) screens in protoplast assays⁵³. To generate the *amiRNA* expression constructs, candidate *amiRNA* sequences were cloned into the pUC119-RCS plasmid. To generate the target construct for *amiRNA* screens, the coding region of the *FIE* cDNA was PCR amplified and cloned into the plasmid with a heat shock promoter (pHSP) to generate pHSP-FIE-Flag-NOS. The pHBT-GFP-HA plasmid was used as a control for protoplast co-transfection and internal control as described⁵³. After screening in protoplast, the optimal *amiRNA* was amplified and transferred to the oestradiol-inducible vector pLB12 (ref.⁵⁴). Positive transformants were selected based on kanamycin resistance.

For the PUP-IT proximity-tagging system²⁷ (for Fig. 2a,b), the sequences of p2X35S-3×Flag-pup (E) and pUBQ10-PafA-HA were synthesized and inserted into the pCAMBIA1300 binary vector, resulting in *pCambia-PUP-IT*. The sequence encoding the C terminus (1226–2480) of TOR (*TOR-C*) was amplified by PCR to generate the plasmid with pUBQ10-TOR-C-PafA-HA and p2X35S-3×Flag-pup (E). The coding region sequences of PRC2 components, including *CLF*, *SWN*, *EMF2*, *VRN2*, *FIE* and *MSI1*, were amplified by PCR and cloned into the pHBT-MYC plant expression vector⁵⁵. For the confocal imaging of FIE mutants in mesophyll protoplasts, the coding region of *FIE* was first amplified by PCR and cloned into the pHBT-GFP expression vector, resulting in pHBT-GFP-FIE. The mutant variants were generated by site-directed mutagenesis using pHBT-GFP-FIE as a template. For the expression of recombinant FIE protein and its mutant variant proteins in *Escherichia coli*, the coding region of *FIE* was first amplified by PCR and cloned into the pET14b expression vector, resulting in pET14b-FIE. The mutant variants were generated by site-directed mutagenesis using pET14b-FIE as a template. We produced the recombinant protein for each of four core subunits of the plant PRC2 complexes using the SF9 insect cells. The coding sequences of *FIE* and its phosphorylation site mutation SSTS/AAAA with 3×Flag tags at the N terminus were cloned into the pFastBac1 vector. The coding sequences of the other PRC2 subunits *CLF*, *EMF2* and *MSI1* were cloned into the pFastBac1 vector with His tags at their N terminus. All constructs were verified by Sanger sequencing. The primers used for plasmid construction and site-directed mutagenesis are listed in Supplementary Table 8.

Plant materials

The *A. thaliana* ecotype Columbia (Col-0) was used as wild-type (WT) plants in this study, unless otherwise stated. The oestradiol-inducible RNAi *tor-es* mutant and the *S6K1-HA* transgenic line have been described previously²¹. The transgenic plants expressing PRC2 components, pSWN:SWN-GFP⁵⁶, p35S:GFP-CLF⁵⁷, pEMF2:EMF2-GFP⁵⁸ and pMSI1:MSI1-GFP⁵⁸ have been described previously. The T-DNA null

mutants in canonical TORC1, including *raptor1* (SALK_078159)²⁴, *raptor2* (SALK_043920)²⁴, *lst8-1-2* (SAIL_641_D10)²⁵ and *lst8-2* (SALK_018605), were confirmed by genotyping and RT-qPCR. Transgenic plants *GFP-FIE/fie*, *SSTS/AAAA/fie* and *fie-amiR-es* were generated as described below. Col-*FRI*^{SF2} (Col-*FRI*)⁴² and pFLC:FLC-GUS in Ler-*FRI*⁵⁹ lines were used for the vernalization analysis. The pFIE:Flag-GFP-FIE construct was introduced into Col-*FRI*, *tor-es* or *fie-amiR-es* by genetic crossing, antibiotic selected, and confirmed by PCR-based genotyping and immunoblot analyses. Col-*FRI* was crossed with S6K1-HA, *tor-es*, *GFP-FIE/fie* or *SSTS/AAAA/fie* and confirmed by PCR-based genotyping and immunoblot analyses. The pKNAT1:GUS⁶⁰ line was introduced into *GFP-FIE/fie* and *SSTS/AAAA/fie* by genetic crossing and confirmed by PCR-based genotyping.

Plant growth conditions

Seeds were surface sterilized with 70% ethanol and bleach (25% bleach, 0.02% Triton X-100 for 10 min), washed with sterile water three times, and stratified at 4 °C for three days before plating. Sterilized seeds were planted and germinated in a nutrient rich sugar-containing medium, liquid 0.5× MS medium (0.5× MS, 2 mM MES and 0.5% sucrose, pH 5.7) or on solid 0.5× MS medium (0.5× MS, 2 mM MES, 0.5% sucrose and 0.6% phytoagar, pH 5.7). To analyse the effect of TOR activity on plant growth and development (for Fig. 1a and Extended Data Fig. 1a,b), Torin2 at indicated concentrations (0, 0.1, 0.5, 1, 5 and 10 μM), 10 μM oestradiol, or DMSO only, were added at the time of seed germination for 8 days. To quantify the histone methylation marks and gene expressions in WT and the *tor-es* mutant (for Fig. 1b,c and Extended Data Figs. 1a–d, 3b and 8d,e), seeds were planted and germinated in liquid 0.5× MS medium (0.5× MS, 2 mM MES, and 0.5% sucrose, pH 5.7) for 7 days. On the fourth day, 10 μM oestradiol was added to the medium to deplete TOR in *tor-es* plants. For the sugar starvation experiment (for Fig. 1d,e and Extended Data Figs. 2e and 8f,g), WT, S6K1-HA or the indicated mutant *Arabidopsis* seedlings were grown in sugar-free liquid 0.5× MS medium (0.5× MS, 2 mM MES, pH 5.7) for 7 days. The endogenous glucose from the seed is depleted three days after germination⁴. Glucose (25 mM) was added on the eighth day for the indicated time (for Fig. 1d,e) or 6 h (for Extended Data Figs. 2e and 8f,g) to stimulate TOR signalling. For the experiments with TOR or S6K inhibitors (for Fig. 1f,g and Extended Data Fig. 2a–d), WT or S6K1-HA seedlings were grown in liquid 0.5× MS (with 0.5% sucrose, PH 5.7) medium for four days and treated with DMSO as the control or 10 μM of different chemical inhibitors that target TOR or S6K for three days. Unless otherwise indicated, plants were grown at 23/20 °C, 12 h/12 h light/dark, 60% relative humidity and 75 μmol m^{−2} s^{−1} light.

External data sources

The sequences of proteins were obtained from TAIR (<https://www.arabidopsis.org/>) and NCBI (<https://www.ncbi.nlm.nih.gov/>). The 3D protein structures were predicted by RaptorX (<http://raptorg.uchicago.edu/>).

Generation, purification and application of the pFIE(S14) antibody

The phospho-site-specific anti-pFIE(S14) antibody was custom-made by ABclonal. In brief, a phosphopeptide (NESIVGpSLTPSN-C) was synthesized and conjugated to keyhole limpet haemocyanin carrier for the immunization of four rabbits. The polyclonal antiserum was first affinity-purified using the phosphopeptide, and the elution was then passed over the column coupled with the non-phospho-peptide (NESIVGSLTPSN-C) to remove nonspecific antibodies⁶¹. The pFIE(S14) antibody was first tested by dot blot assays against the phospho- and non-phospho-peptides. The anti-pFIE(S14) antibody was further validated by immunoblot analyses against the His-FIE or His-FIE(S14A) proteins without or with TOR phosphorylation after the in vitro kinase assay.

To detect the phosphorylated pFIE(S14) in vivo, pFIE(S14) antibody was used to detect the Flag-GFP-FIE protein immunoprecipitated from

transgenic plants by immunoblot analyses. Specifically, *GFP-FIE/fie* or *tor-es* seedlings expressing Flag–GFP–FIE were grown in liquid 0.5× MS (with 0.5% sucrose, pH 5.7) medium for eight days (for Fig. 2g). The medium was changed to liquid 0.5× MS without sugar and the seedlings were starved in dark for two days. Glucose (25 mM) was added to the medium for 2 h to stimulate TOR activity. To deplete TOR, *tor-es* seedlings were induced by 10 µM β-oestradiol for four days. For Torin2 treatment, 2 µM Torin2 was added into the medium one day before collecting the samples. To examine glucose-induced FIE phosphorylation (for Fig. 2h and Extended Data Fig. 5d), *GFP-FIE/fie* seedlings were grown in sugar-free liquid 0.5× MS medium (0.5× MS, 2 mM MES, pH 5.7) for 7 days. Glucose (25 mM) was added to the medium for 2 h on the 8th day to stimulate TOR signalling.

Approximately 5 g (about 1,000) seedlings were collected and ground to fine powder with a mortar and pestle in liquid nitrogen and suspended in 5 ml of extraction buffer (25 mM Tris-HCl pH 7.6, 150 mM NaCl, 5 mM EDTA, 10 mM *p*-nitrophenyl phosphate, 20 mM β-glycerophosphate, 10 mM sodium pyrophosphate, 2 mM Na₃VO4, 1 mM NaF, 1% NP-40, 10% glycerol, 1× protease inhibitor cocktail tablet, and 1× Phosphatase Inhibitor Cocktail Tablet (PhosSTOP)). The tissues were further homogenized by grinding thoroughly and then centrifuged in an SS34 rotor for 25 min at 12,500 rpm and the supernatant was saved. The pellets were resuspended in 2 ml lysis buffer (25 mM Tris-HCl, pH 7.6, 75 mM NaCl, 5 mM EDTA, 1% Triton X-100, 0.1% SDS, 10 mM *p*-nitrophenyl phosphate, 20 mM β-glycerophosphate, 10 mM sodium pyrophosphate, 2 mM Na₃VO4, 1 mM NaF, 10% glycerol, 1× protease inhibitor cocktail tablet, and 1× Phosphatase Inhibitor Cocktail Tablet (PhosSTOP)) and sonicated for 1 min (10s on, 20s off). The supernatant from the two-step extraction was combined and incubated with 100 µl of pre-washed anti-Flag M2 Agarose Beads (Sigma, A2220) at 4 °C for 2 h with rotation. Beads were washed five times with extraction buffer. Proteins were then eluted from the anti-Flag M2 Agarose beads with 50 µl of 300 mg ml⁻¹ of 3×Flag peptide (Sigma, F4799) five times at room temperature. The elution was precipitated with an equal volume of 20% TCA/acetone and washed with acetone. The pellet was resuspended in 100 µl of 1× calf intestinal alkaline phosphatase (CIP) buffer. For CIP treatment, 50 µl of Flag–GFP–FIE protein solution was mixed with or without (mock) 10 U CIP (New England Biolabs, M0290) for 1 h at 37 °C. The reaction was stopped by adding 2× sample buffer and boiled for 5 min at 95 °C before running the SDS-PAGE. Site-specific phosphorylation was detected by immunoblot analysis with pFIE(S14) antibody at 1:500 dilution in 5% BSA.

RNA extraction and gene expression analysis

Whole seedlings from liquid medium or the aerial parts of plants from the agar plate were collected and frozen in liquid nitrogen. Total RNA was isolated from seedlings ground in liquid nitrogen and extracted using the protocol with the Trizol reagent (Invitrogen). Total RNA (0.5 µg/20 µl reaction) was treated with DNase I (RQ1 RNase-free DNase I, Promega), and converted to cDNA using M-MLV reverse transcriptase (RNase H minus, Point Mutant, Promega) and oligo(dT) primer according to the manufacturer's guidelines. Quantitative PCR was carried out as described⁶² using the primers listed in Supplementary Table 8. The relative gene expression was normalized to the expression of *UBQ10* (*AT4G05320*), *UBC21* (*At5g25760*) or *ACTIN2* (*At5g09810*). A minimum of triplicate biological samples were analysed with consistent results.

To analyse the perturbed global gene expression pattern in the *fie-amiR-es* and *SSTS/AAAA/fie* mutants, RNA-seq analyses were carried out as described⁵¹. Seedlings of WT, *fie-amiR-es*, *GFP-FIE/fie* or *SSTS/AAAA/fie* were grown on 0.5× MS (with 0.5% sucrose, pH 5.7) agar medium for two weeks (For Fig. 3a–e,g and Extended Data Fig. 7a–c). For the inducible *fie-amiR-es* mutant, 10 mM oestradiol was added into the medium at the beginning of germination to induce FIE depletion. The aerial part of plants was collected for RNA extraction at

two weeks. Total RNA (0.5 µg) was used for preparing the library with NEBNext Ultra II RNA Library Prep Kit for Illumina sequencing according to the manufacturer's guidelines. For the DNA fragment enrichment step, the template was amplified by PCR for eight cycles with adaptors of different barcodes. The libraries were sequenced using an Illumina HiSeq4000 at GENEWIZ Next Generation Sequencing centre, and 150 bp paired-end reads were generated.

ChIP analysis

ChIP-seq data were processed and analysed as previously described with minor modification⁶³. In brief, plants (1 g) were ground into fine powder in liquid nitrogen and suspended with 10 ml nuclei isolation buffer (10 mM HEPES pH 8.0, 1 M sucrose, 5 mM KCl, 5 mM EDTA, 0.6% Triton X-100, 0.4 mM PMSF, and fresh protease inhibitor cocktail). The homogenate was incubated with 1% formaldehyde for 15 min and stopped with 125 mM glycine. The extract was filtered through double layers of wet Miracloth and centrifuged at 1,500 g for 10 min at 4 °C. The nuclei pellet was washed 3 times with 10 ml nuclei isolation buffer. The pellet was resuspended in 0.2 ml nuclei lysis buffer (50 mM Tris-HCl pH 8.0, 10 mM EDTA, 1% SDS, and fresh protease inhibitor cocktail) and sonicated for 3 × 10 min, 30s on 30s off at high setting, and then diluted 10-fold to 2 ml with ChIP dilution buffer (1.1% Triton X-100, 1.2 mM EDTA, 16.7 mM Tris-HCl pH 8.0, 167 mM NaCl, and fresh protease inhibitor cocktail). Chromatin was immunoprecipitated with an antibody at 4 °C overnight with rotation. Each antibody, against H3 (Abcam, 1791, 1:1,000), H3K27me3 (Millipore, 07-449, 1:200) and H3K9me2 (Abcam 1220, 1:200), was bound to the pre-washed protein A or G Dyna-beads (40 µl) for 1 h at 4 °C with rotation. The immunoprecipitated chromatin was washed twice with each of the following solutions for 5 min at 4 °C: 1 ml of low-salt buffer, high-salt buffer, LiCl buffer and TE buffer. Protein complexes were eluted from beads with 400 µl of elution buffer (1% SDS and 0.1 M NaHCO₃) at 65 °C for 10 min. The eluted chromatin was reverse crosslinked with 0.2 M NaCl at 65 °C overnight, and treated with RNase A (0.2 mg ml⁻¹) at 37 °C for 1 h, proteinase K at 50 °C for 1 h, and purified with phenol:chlorophorm followed by ethanol precipitation. The enriched DNA was subjected to quantitative PCR (qPCR) analysis or library construction and Illumina sequencing for ChIP-seq analysis.

ChIP-qPCR was performed using the iQ SYBR green supermix (Bio-Rad) and normalized using H3 level as an internal standard. H3K27me3 enrichment is shown as the percentage of H3. Three biological replicates were performed for each experiment. Primer sequences used for ChIP-qPCR are listed in Supplementary Table 8.

To quantitatively compare genome-wide H3K27me3 levels across plant samples, a method called ChIP with reference exogenous genome (ChIP-Rx) was performed with minor modifications as previously described²³. Defined quantities (one-tenth) of the reference chromatin from Human 293T cells were added into *Arabidopsis* chromatin from 1 g of seedlings before immunoprecipitation.

To determinate the concentration of chromatin, 10 µl from 2 ml of *Arabidopsis* chromatin was reverse crosslinked, digested with RNase A and proteinase K, and followed by DNA purification as described above. The concentration of purified DNA was determined using Qubit dsDNA High-Sensitivity Assays (Invitrogen). The DNA concentration of 10 µl chromatins from 10⁶ human HEK293T cells was also isolated and determined with the same method. One-tenth of human chromatin (about 10 µg DNA) compared with the *Arabidopsis* chromatin was mixed with each of different *Arabidopsis* samples (about 100 µg DNA) before immunoprecipitation. Purified DNA (5 ng) after ChIP was used for preparing the library with NEBNext Ultra II DNA Library Prep Kit for Illumina according to the manufacturer's guidelines. For the DNA fragments enrichment step, the templates were amplified for eight cycles with adaptors of different barcodes. The libraries were sequenced using an Illumina HiSeq4000 at GENEWIZ Next Generation Sequencing centre and 150 bp pair-end reads were generated.

In vivo co-immunoprecipitation assay

To capture the dynamic interaction between TOR kinase and substrates in vivo, TOR activity was synchronized and stimulated by starvation and glucose depletion, and formaldehyde crosslinking was applied to stabilize the TOR-substrate interaction. Specifically, transgenic *Arabidopsis* seedlings expressing Flag–GFP–FIE or Col-0 seedlings as the control were grown in liquid 0.5× MS (with 0.5% sucrose, pH 5.7) medium for eight days (for Fig. 2c). Then the liquid medium was changed to 0.5× MS without sugar and the seedlings were starved in dark for 3 days. Glucose (25 mM) was added into the medium for 2 h to stimulate TOR activity. To test the effect of glucose concentration on the interaction between TOR and FIE (Extended Data Fig. 4a), transgenic seedlings expressing Flag–GFP–FIE were grown in sugar-free liquid 0.5× MS medium (0.5× MS, 2 mM MES, pH 5.7) for 7 days. Different concentration of glucose (0, 0.1, 0.5, 1, 5, 10, 20 and 25 mM) were added to the medium for 2 h on the eighth day to stimulate TOR signalling. Whole seedlings were crosslinked in 1% formaldehyde for 15 min and collected after removing all the liquid with Kimwipes. Crosslinked plants were ground into powder with liquid nitrogen and suspended in extraction buffer (25 mM Tris-HCl pH 7.6, 150 mM NaCl, 5 mM MgCl₂, 10% glycerol, 0.1% NP-40, 0.5 mM DTT, and fresh protease inhibitor cocktail). After centrifugation at 18,000 rpm in a microfuge at 4 °C for 20 min, the supernatant was incubated with pre-washed anti-Flag M2 Agarose Beads (Sigma, A2220) at 4 °C for 2 h with rotation. Beads were washed five times with extraction buffer. Protein complexes were eluted twice with 3×Flag peptide. The eluted and input samples were mixed with 2X sample buffer and boiled for 10 min at 95 °C before SDS-PAGE and immunoblot analysis.

Protein expression and purification

Recombinant proteins were expressed in *E. coli* Rosetta 2 (DE3) pLysS Cells (Novagen). *E. coli* cells transfected with expression plasmids were first grown in 80% LB/20% TB medium with ampicillin (100 µg ml⁻¹) at 37 °C until reaching 0.6 OD₆₀₀. The cell culture was cooled to 18 °C and protein expression was induced with 0.5 mM isopropyl β-D-1-thiogalactopyranoside for 18 h. Cells were collected, resuspended in lysis buffer (50 mM pH 7.4 HEPES, 300 mM NaCl, 20 mM imidazole, and fresh protease inhibitor cocktail), and lysed by sonication. The supernatants were incubated with Ni-NTA agarose (Qiagen) for 2 h at 4 °C. The Ni-NTA agarose was washed four times with washing buffer (50 mM pH 7.4 HEPES, 300 mM NaCl, 40 mM imidazole). The recombinant protein was eluted with elution buffer (50 mM pH 7.4 HEPES, 300 mM NaCl, 250 mM imidazole, and fresh protease inhibitor cocktail) for 10 min at room temperature and concentrated by Amicon Ultra-15 10K filter (Millipore). Proteins were stored at -80 °C after being flash-frozen in liquid nitrogen.

Histone methyltransferase assays with purified PRC2 complexes

Each of the four core components of the *Arabidopsis* PRC2 complexes, including CLF, EMF2, MSI1, and FIE (WT or SSTS/AAAA mutant) were expressed in insect Sf9 cells using the standard Bac-to-Bac baculovirus expression system (Invitrogen). The Sf9 cells were infected with equal amounts of baculovirus for expressing each subunit at the density of 1.8 × 10⁶ cells per ml. The cells were collected and frozen with liquid nitrogen after 72 h incubation at 130 rpm at 27 °C. Insect cells were resuspended in lysis buffer (20 mM HEPES at pH 7.9, 300 mM KCl, 1.5 mM MgCl₂, 1 mM PMSF, 0.5 mM DTT, and 0.1% Triton X-100), and sonication 10 × 20 s on ice. After centrifugation at 18,000 rpm in a microfuge at 4 °C for 20 min, the supernatant was incubated with pre-washed anti-Flag M2 Agarose Beads (Sigma, A2220) at 4 °C for 2 h with rotation. Beads were washed five times with extraction buffer. Protein complexes were eluted twice with 3×Flag peptide at room temperature. The protein buffer was changed to storage buffer (20 mM HEPES at pH 7.9, 300 mM KCl, 1.5 mM MgCl₂, 10% glycerol) and concentrated by Amicon Ultra-15 10K filter (Millipore). Proteins were stored at -80 °C after being

flash-frozen in liquid nitrogen. The Histone lysine methyltransferase assay was performed as previously described⁶⁴. In brief, 0.3 µg of recombinant PRC2 complexes (with WT or SSTS/AAAA mutant form of FIE) were incubated with 1 µg of H3 (New England Biolabs, M2503S) in the reaction buffer (20 mM HEPES at pH 7.9, 2 mM MgCl₂, 1 mM DTT, and 10 µM SAM) for 2 h at 30 °C. The reaction was stopped by addition of 4× loading dye and heated for 5 min at 95 °C. The quantitative level of H3K27me3 was detected by immunoblot analyses using specific anti-H3K27me3 antibody as described above.

TOR kinase assay

In vitro TOR kinase assay was performed as previously described⁴. To immunoprecipitate the endogenous TOR complexes, WT seeds were germinated and grown in liquid medium (0.5× MS, 0.5% sucrose, pH 5.7, 6 seedlings in 1 ml in each well in 6-well plates) for 7 days. The same fresh medium (1 ml) was replenished for 2 more h to maximize TOR activity. TOR complexes purified from six seedlings could be used for ten kinase reactions. For in vitro kinase assay (for Fig. 2d,f and Extended Data Fig. 4h), 1 µg of His–FIE or the mutant proteins were incubated with the immunoprecipitated TOR kinase on the beads in the kinase buffer (25 mM HEPES, pH 7.4, 50 mM KCl, 10 mM MgCl₂, 1 mM DTT, 10 µM cold ATP, 2 µCi [γ -³²P]-ATP) at 30 °C for 30 min with shaking at 1,000 rpm. For TOR inhibitor treatment, the immunoprecipitated TOR kinase on the beads was pre-incubated with 1 µM Torin2 for 10 min at room temperature before the kinase assay. The reaction was stopped by adding 2× SDS-PAGE loading buffer. After SDS-PAGE and subsequent gel drying, protein phosphorylation was visualized by autoradiography using the Typhoon imaging system (GE Healthcare).

Tandem mass spectrometry analysis

To identify the TOR phosphorylation sites in FIE, 5 µg of His–FIE recombinant proteins were subjected to in vitro TOR kinase assay in the kinase buffer for 2 h at 30 °C. The phosphorylated His–FIE was separated by 10% SDS-PAGE gel. The gel was stained with Thermo GelCode Blue Safe Protein Stain and destained with ddH₂O. The His–FIE band was excised and subjected to in-gel digestion with trypsin. The phospho-peptides were enriched using the TiO₂/ZrO₂ media from Glygen⁶⁵ and subjected to LC-MS/MS analysis using the Orbitrap Fusion Tribrid mass spectrometer (Thermo Scientific)⁶⁶. The raw data of LC-MS/MS spectra was analysed by the Mascot search engine (version 2.2, Matrix Science). The parameters were: *Arabidopsis* TAIR10 database (32,785 entries, <https://www.arabidopsis.org/>), precursor mass tolerance at 10 ppm, fragment mass tolerance at 0.8 Da, trypsin with one missed cleavage, oxidation (M) and phosphorylation (S, T, Y) as dynamic modifications. The identified phosphorylated peptides and each phosphorylation site assignment were confirmed by manual inspection of the precursor mass and fragmentation ions. To validate the FIE phosphorylation sites from in vivo immunoprecipitation using Flag antibody, the Flag–GFP–FIE protein was immunoprecipitated from 100 g transgenic seedlings at 8 days as described above (for Fig. 2e and Extended Data Fig. 4b). The Flag–GFP–FIE protein was separated and excised from a SDS-PAGE gel and subjected to in-gel digestion with trypsin. The phosphopeptides were enriched and analysed using the same LC-MS/MS method, except that targeted precursor ions and charge states (+2 and +3) were put in the inclusion list for targeted MS/MS acquisition. The accurate precursor mass and corresponding MS/MS spectra were validated using the synthetic phosphopeptide.

Protoplast assays for microscopy detection, PUP-IT and amiRNA screening

Mesophyll protoplasts were isolated from four-week-old WT leaves and transfected essentially as described⁶⁷. For the PUP-IT proximity-tagging system (for Fig. 2a,b), protoplasts (2 × 10⁵) in 1 ml MMg (0.4 M mannitol, 15 mM MgCl₂, 4 mM MES, pH 5.7) were co-transfected with 100 µg of pUBQ10-TOR-C-PafA-HA-p2X35S-3×Flag-pup (E) and 100 µg of

HBT-PRC2-MYC expressing different PRC2 components. Transfected protoplasts were incubated in 5 ml WI (0.5 M mannitol, 20 mM KCl, 4 mM MES, pH 5.7) in a 10 cm plate at room temperature for 12 h. The protoplast pellet was lysed in 1 ml extraction buffer (25 mM Tris-HCl pH 7.6, 150 mM NaCl, 5 mM MgCl₂, 10% glycerol, 0.1% NP-40, 0.5 mM DTT, and fresh protease inhibitor cocktail) with 0.1% SDS and subjected to immunoprecipitation using anti-Flag M2 Agarose Beads (Sigma, A2220) as described above. The input and immunoprecipitated proteins were mixed with 2× sample buffer and boiled for 10 min at 95 °C before gel electrophoresis and immunoblot analysis. For the confocal imaging of FIE and mutant proteins in mesophyll protoplasts (for Extended Data Fig. 5f), 200 µl protoplasts (4×10^4) were co-transfected with 38 µg of plasmid DNA to expression GFP-FIE or various mutants and 2 µg of pHBT-HY5-mCherry to express HY5-mCherry as a control for protoplast co-transfection and nuclear localization. Transfected cells were incubated in 1 ml WI in a 6-well plate at room temperature for 10 h before imaging with a Leica TCS SP8 laser scanning confocal microscopy (Leica). For optimal amiRNA screening (for Extended Data Fig. 7a), 200 µl protoplasts (4×10^4) were co-transfected with 35 µg of plasmid DNA expressing each candidate *amiRNA* (the empty *amiRNA* expression plasmid served as a control), 4 µg of pHSP-FIE-Flag plasmid, and 1 µg pHBT-GFP-HA plasmid (as a transfection internal control). Transfected cells were incubated in WI in a 6-well plate at room temperature for 3 h before the heat shock pulse at 37 °C for 1 h. Protoplasts were collected for immunoblot analysis after three more hours of incubation at room temperature.

Vernalization treatment

For all the vernalization experiments (for Fig 4, Extended Data Fig. 9), plants were in or crossed into the *FR1^{s2}*(Col-*FR1* or Ler-*FR1*) background⁴². Plants were grown on solid 0.5× MS (pH 5.7) medium (30 ml medium, 35 seedlings in 100 mm plates) or in liquid 0.5× MS (with 0.5% sucrose, pH 5.7) medium (1 ml medium, 6 seedlings in each well in 6-well-plates, or 10 ml medium, 50 seedlings in 100 mm plates) for chemical treatments under a 12 h light/12 h dark photoperiod condition at 23 °C/20 °C. For chemical treatments and GFP imaging (Fig. 4b–e and Extended Data Fig. 9a–d), liquid medium was used for more effective chemical penetration and handling intact roots for confocal imaging. For the other experiments, solid medium was used (Fig. 4a,h–j and Extended Data Fig. 9e). For glucose measurement, the results were more consistent using the solid medium for fresh weight measurement and tissue grinding. It was much easier to select the *SSTS/AAAA*/*fie* mutant when grown on a solid medium (Fig. 4i,j and Extended Data Fig. 9e). Notably, the results for gene expression and H3K27me3 dynamic during vernalization were similar when using liquid (Fig. 4b,e Extended Data Fig. 9b) or solid medium (Fig. 4i,j and Extended Data Fig. 9e). Plant samples collected at 8 days before vernalization were referred as NV. Seedlings were vernalized from the 8th day under an 8h light/16h dark short-day condition at 4 °C with 60% relative humidity and 40 µ mol m⁻² s⁻¹ light for 40 days (V), and then transferred back to the normal temperature condition (T) for seven more days for sample collection. For the *tor-es* mutant with the Col-*FR1*/background, 10 µM oestradiol was added into the medium three days before vernalization. For Torin2 and INK128 treatment, 1 µM inhibitor was added in the medium one day before vernalization. Plant samples were collected every ten days during cold treatment, and medium with oestradiol or inhibitors were also refreshed every ten days. Collected samples were subjected to RNA expression quantification by RT-qPCR analysis and H3K27me3 quantification by ChIP-qPCR analysis. For glucose measurement during vernalization, plant materials were washed twice with cold water and frozen after removing all the liquid with Kimwipes. The glucose level was measured using the Glucose Assay Kit (Colorimetric) according to the manufacturer's guidelines. For GUS histochemical staining, *pFLC:FLC-GUS* (Ler-*FR1*) seedlings before and after 40 days of vernalization were collected and stained essentially as described⁶⁸. Flowering time was measured by counting rosette leaves at the time of bolting.

Protein blot analysis

Plants were collected, frozen and ground into fine powder with a blue pestle in liquid nitrogen in a microfuge tube. For total protein extract, an equal volume of 2× SDS-PAGE protein loading buffer was added to each sample and boiled for 10 min. To detect histone proteins, nuclear extract enriched with histone was prepared as described⁶⁹ and denatured by boiling in protein loading buffer. After centrifugation, the supernatant of each protein sample was separated by SDS-PAGE and transferred to the PVDF membrane for immunoblot analysis. Protein blots were probed using antibodies against TOR (1:1,000)²¹, pFIE(S14) (1:500), pS6KI(T449) (1:500)²¹, RPS6 (ref.⁷⁰) (1:5,000), pRPS6(S237) (1:3,000), pRPS6(S240)⁷¹ (1:3,000), H3 (Abcam, ab1791, 1:5,000), H3K4me3 (Abcam, ab8580, 1:1,000), H3K9me2 (Abcam 1220, 1:1,000), H3K27me3 (Millipore, 07-449, 1:1,000), H3K36me3 (Abcam, ab9050, 1:1,000), tubulin (Sigma, T6199, 1:5,000), GFP (CLONTECH, 632381, 1:5,000), HA-HRP (Sigma, L2013819001, 1:5,000), Flag-HRP (Sigma, A8592, 1:5,000), and MYC-HRP (Roche, 1-814-150, 1:1,000), Anti-Mouse IgG-HRP (Sigma, A4416, 1:5000), Anti-Rabbit IgG-HRP (Sigma, A0545, 1:5,000). The signal intensity of each blot was quantified by ImageJ.

Confocal microscopy

Transgenic plants expressing various GFP fusion proteins were grown in liquid 0.5× MS medium with 0.5% sucrose, pH 5.7 (for Fig 2i,j and Extended Data Fig. 6c,d). Transgenic plants expressing GFP-FIE or GFP-FIE(SSTS/AAAA) were grown without treatment for 4 days for image acquisition of leaf primordia and root elongation and root meristem zones. For TOR inhibitor treatment, plants were grown for 4 days and treated with 10 µM Torin2 or AZD8055 for 24 h before imaging. For plants in the *tor-es* mutant background, 10 µM oestradiol was added to the medium at the second day and incubated for 3 days before the image acquisition. For quantitative imaging of the dynamic GFP-FIE C/N ratio under sugar starvation, plants were germinated and grown in liquid 0.5× MS medium without sugar. Pictures were taken every day from day 2 to 6 (Extended Data Fig. 6f,g). For sugar starvation and glucose stimulation experiments (Extended Data Fig. 6h–j and Supplementary Video), plants were grown in liquid 0.5× MS medium without sugar for 5 days before glucose (25 mM) stimulation for 6 h before imaging. Plants for imaging were transferred into 35 mm glass bottom dish with 20 mm micro-well filled with 300 µl liquid 0.5× MS medium with 25 mM glucose and immediately used for time-lapse live imaging with 10 min intervals for 6 h. For imaging GFP-FIE and GFP-tagged FIE variants in protoplasts, transfected cells as previously described⁶⁷ were incubated at room temperature for 10 h before imaging.

Confocal images were acquired using the Leica Application Suite X software on a Leica TCS SP8 (Leica) confocal microscope with the 20× objective lens for roots and protoplasts or the 40× water lens for leaf primordia. The scanning resolution was set to 1,024 Å × 1,024 or 2,048 Å × 2,048 pixels. To obtain fluorescence images of roots and protoplasts, the excitation was set at 488 nm (GFP) or 587 nm (mCherry) and emission at 494–541 nm (GFP) or 595–625 nm (mCherry). To obtain fluorescence images of leaf primordia, GFP and autofluorescence were visualized by excitation at 488 nm using the argon laser and emission at 510–520 nm (GFP) or 660–680 nm (autofluorescence). The auto-fluorescence signal was removed by applying the Channel and Spectral Dye Separation tool (Leica). For time-lapse live imaging, images were captured every 10 min for 6 h and replayed as a video. The images were collected and processed using Adobe Photoshop software. Quantification of subcellular localization of GFP-FIE were performed using LAS-X (Leica Application Suite v. X3.1.1.15751, Wetzlar, Germany). The GFP fluorescence intensity from the whole-cell and nuclear areas was measured. The fluorescence of the nuclear area was considered as GFP-FIE in the nucleus (N), and the fluorescence in the cytosol (C) was determined by subtracting the nucleus from the entire cell. The relative GFP fluorescent intensity between the cytosol (C) and nucleus (N) was

Article

analysed and presented as the quantitative C/N ratio from more than 15 cells in three biological replicates.

Processing and analysis of the ChIP-seq data

ChIP-seq data were processed and analysed as previously described⁷². In brief, the quality of each sequencing library was assessed by examining fastq files with FastQC (version 0.11.5). Then, sequencing adaptors were removed using Trimmomatic (version 0.36)⁷³. The Sickle program was used to eliminate bases with low quality scores (<20) and short reads (length < 20). The remaining clean reads were aligned to the reference sequence. The ChIP-seq reads were mapped to *Arabidopsis* (TAIR10) and human (hg19) combined genomes, using BWA-MEM (version 0.7.15-r1142-dirty). Moreover, the view function of samtools (version 1.6) was used to remove reads with quality (Q) < 20 ($Q = -10\log_{10}(p)$, where p is an estimate of the probability that the alignment does not correspond to the read's true point of origin). The rmdup function of samtools (version 1.6) was used to remove duplicated reads mapped to exactly the same position because they were considered to be artifacts caused by PCR during the library construction step. The number of reads mapped to human genome was used to calculate reference derived normalization factor as previously described²³. MACS2⁷⁴ utility callpeak was used to identify read-enriched regions (peaks) and utility pileup was used to generate bedgraph files with default settings. The number of reads in the bedgraphs was then scaled by the reference derived normalization factor to generate RRPM. The bedGraphToBigWig (version 4) of UCSC was used to transfer bedgraph files to bigwig files, and then the bigwig files were loaded onto JBrowse⁷⁵ (version 1.12.1) for data visualization. Target genes were defined as genes with a peak within or near the gene body (± 2 kb). For profiling the modification surrounding peak summits, regions from 2 kb upstream and 2 kb downstream of peak summits were divided into 40 tiles in total (20 upstream tiles and 20 downstream tiles), the RRPM value in each tile of each peak was used to plot heat map and the average RRPM value in each tile was used to make a line plot.

Processing and analysis of the RNA-seq data

The RNA-seq reads were mapped to the *Arabidopsis* (TAIR10) genome with HISAT2⁷⁶ program (version 2.1.0). The featureCount program of Subread⁷⁷ package (version 1.5.3) was used to quantify the RNA-seq expression levels of the TAIR10 annotated gene models. DESeq2 (ref.⁷⁸) was used to determine the significance of the differential expression between samples with the combined criteria: $|log_2 \text{fold change}| \geq 1$ and $FDR \leq 0.05$. We added a pseudocount of 0.01 to DESeq2 normalized expression values to recalculate $\log_2 \text{fold change}$, which helped us avoid infinite values resulting from zero counts and seek some differentially expressed genes with relative low counts.

Gene ontology term enrichment analysis

The gene ontology (GO) term enrichment analysis was performed using The TAIR GO term enrichment tool BiNGO (<http://www.psb.ugent.be/cbd/papers/BiNGO/Home.html>)⁷⁹. In brief, we first compiled the genes that are targeted by H3K27me3 and upregulated in STSS/AAAA/fie (Supplementary Table 5). Next, Fisher's exact test ($FDR < 0.05$) was used by the website to identify GO terms that are significantly over-represented with the compiled gene list. Genes from 'not assigned' group were manually checked to identify the ones related to 'regulation of transcription, DNA-templated (GO:0006355)'. The categories in biological process with fold enrichment > 2 and $FDR < 10^{-10}$ were selected and presented in Extended Data Fig. 8b and Supplementary Table 6.

Chemical inhibitors for TOR kinase and S6K

The ATP-competitive chemical inhibitors for both mTORC1 and mTORC2, Torin2, AZD8055, INK128, WYE132 and WYE345, were tested empirically for efficacy in intact *Arabidopsis* seedlings and used in this study^{2,15,80–85}. The second-generation ATP-competitive TOR kinase

inhibitors, Torin2 and INK128, have been examined by genome-wide selectivity profiles to ensure the specificity for TOR kinase inhibition^{80–82}, and INK128 was shown to be effective in mammalian culture cells and in mice⁸². Torin2 was used for the initial chemical screens in seedlings up to 8-d treatment at different concentrations because Torin2 shows slower dissociation from TOR kinase and is more effective in sustained blocking of mTOR1 and mTORC2-mediated pAKT(S473) than AZD8055 in human cells⁸⁴ and in *Arabidopsis* seedlings¹⁵. Chemical inhibitors for S6K, staurosporin and PF-4708671, were previously described^{4,86}.

Statistics

For most of the quantitative data shown in this paper represent mean \pm s.d. from at least three biological replicates. Statistical analyses were performed with GraphPad Prism 9 software. Unless otherwise specified, statistical significance was determined with the unpaired two-tailed Student's *t*-test when comparing two groups and one-way or two-way ANOVA when comparing more than two groups with Tukey's multiple comparisons test. The exact P values are indicated in the figures.

Reporting summary

Further information on research design is available in the Nature Research Reporting Summary linked to this article.

Data availability

Sequencing data have been deposited to the Gene Expression Omnibus under accession GSE161807. The pCambia-PUP-IT vector was deposited to Addgene (#186478). The plasmids and the transgenic *Arabidopsis* seeds generated in this study are available upon request. Source data are provided with this paper.

Code availability

Analysis codes are available upon reasonable request from the corresponding authors. No custom codes were central to the conclusions of the paper.

51. Wang, H. et al. *Arabidopsis* flower and embryo developmental genes are repressed in seedlings by different combinations of Polycomb group proteins in association with distinct sets of cis-regulatory elements. *PLoS Genet.* **12**, e1005771 (2016).
52. Clough, S. J. & Bent, A. F. Floral dip: a simplified method for Agrobacterium-mediated transformation of *Arabidopsis thaliana*. *Plant J.* **16**, 735–743 (1998).
53. Li, J. F. et al. Comprehensive protein-based artificial microRNA screens for effective gene silencing in plants. *Plant Cell* **25**, 1507–1522 (2013).
54. Brand, L. et al. A versatile and reliable two-component system for tissue-specific gene induction in *Arabidopsis*. *Plant Physiol.* **141**, 1194–1204 (2006).
55. Liu, K. H. et al. Discovery of nitrate-CPK-NLP signalling in central nutrient-growth networks. *Nature* **545**, 311–316 (2017).
56. Shu, J. et al. Genome-wide occupancy of histone H3K27 methyltransferases CURLY LEAF and SWINGER in *Arabidopsis* seedlings. *Plant Direct* **3**, e00100 (2019).
57. Schubert, D. et al. Silencing by plant Polycomb-group genes requires dispersed trimethylation of histone H3 at lysine 27. *EMBO J.* **25**, 4638–4649 (2006).
58. de Lucas, M. et al. Transcriptional regulation of *Arabidopsis* Polycomb Repressive Complex 2 coordinates cell-type proliferation and differentiation. *Plant Cell* **28**, 2616–2631 (2016).
59. Angel, A., Song, J., Dean, C. & Howard, M. A Polycomb-based switch underlying quantitative epigenetic memory. *Nature* **476**, 105–108 (2011).
60. Ori, N., Eshed, Y., Chuck, G., Bowman, J. L. & Hake, S. Mechanisms that control knox gene expression in the *Arabidopsis* shoot. *Development* **127**, 5523–5532 (2000).
61. Arur, S. & Schedl, T. Generation and purification of highly specific antibodies for detecting post-translationally modified proteins *in vivo*. *Nat. Protoc.* **9**, 375–395 (2014).
62. Niu, Y. & Sheen, J. Transient expression assays for quantifying signaling output. *Methods Mol. Biol.* **876**, 195–206 (2012).
63. Yamaguchi, N. et al. Chromatin immunoprecipitation from *Arabidopsis* tissues. *Arabidopsis Book* **12**, e0170 (2014).
64. Jacob, Y. et al. Selective methylation of histone H3 variant H3.1 regulates heterochromatin replication. *Science* **343**, 1249–1253 (2014).
65. Zhang, T., Schneider, J. D., Zhu, N. & Chen, S. Identification of MAPK substrates using quantitative phosphoproteomics. *Methods Mol. Biol.* **1578**, 133–142 (2017).
66. Pang, Q. et al. Proteomics and phosphoproteomics revealed molecular networks of stomatal immune responses. *Planta* **252**, 66 (2020).

67. Yoo, S. D., Cho, Y. H. & Sheen, J. *Arabidopsis* mesophyll protoplasts: a versatile cell system for transient gene expression analysis. *Nat. Protoc.* **2**, 1565–1572 (2007).
68. Cervera, M. Histochemical and fluorometric assays for uidA (GUS) gene detection. *Methods Mol. Biol.* **286**, 203–214 (2005).
69. Ye, R. et al. Cytoplasmic assembly and selective nuclear import of *Arabidopsis* Argonaute4/siRNA complexes. *Mol. Cell.* **46**, 859–870 (2012).
70. Chen, G. H., Liu, M. J., Xiong, Y., Sheen, J. & Wu, S. H. TOR and RPS6 transmit light signals to enhance protein translation in deetiolating *Arabidopsis* seedlings. *Proc. Natl Acad. Sci. USA* **115**, 12823–12828 (2018).
71. Enganti, R. et al. Phosphorylation of ribosomal protein RPS6 integrates light signals and circadian clock signals. *Front. Plant Sci.* **8**, 2210 (2017).
72. Li, Z. et al. The bread wheat epigenomic map reveals distinct chromatin architectural and evolutionary features of functional genetic elements. *Genome Biol.* **20**, 139 (2019).
73. Bolger, A. M., Lohse, M. & Usadel, B. Trimmomatic: a flexible trimmer for Illumina sequence data. *Bioinformatics* **30**, 2114–2120 (2014).
74. Zhang, Y. et al. Model-based analysis of ChIP-Seq (MACS). *Genome Biol.* **9**, R137 (2008).
75. Buels, R. et al. JBrowse: a dynamic web platform for genome visualization and analysis. *Genome Biol.* **17**, 66 (2016).
76. Kim, D., Langmead, B. & Salzberg, S. L. HISAT: a fast spliced aligner with low memory requirements. *Nat. Methods* **12**, 357–360 (2015).
77. Liao, Y., Smyth, G. K. & Shi, W. The Subread aligner: fast, accurate and scalable read mapping by seed-and-vote. *Nucleic Acids Res.* **41**, e108 (2013).
78. Love, M. I., Huber, W. & Anders, S. Moderated estimation of fold change and dispersion for RNA-seq data with DESeq2. *Genome Biol.* **15**, 550 (2014).
79. Maere, S., Heymans, K. & Kuiper, M. BiNGO: a Cytoscape plugin to assess overrepresentation of gene ontology categories in biological networks. *Bioinformatics* **21**, 3448–3449 (2005).
80. Liu, Q. et al. Discovery of 9-(6-aminopyridin-3-yl)-1-(3-(trifluoromethyl)phenyl)benzo[h][1,6]naphthyridin-2(¹H)-one (Torin2) as a potent, selective, and orally available mammalian target of rapamycin (mTOR) inhibitor for treatment of cancer. *J. Med. Chem.* **54**, 1473–1480 (2011).
81. Liu, Q. et al. Selective ATP-competitive inhibitors of TOR suppress rapamycin-insensitive function of TORC2 in *Saccharomyces cerevisiae*. *ACS Chem. Biol.* **7**, 982–987 (2012).
82. Hsieh, A. C. et al. The translational landscape of mTOR signalling steers cancer initiation and metastasis. *Nature* **485**, 55–61 (2012).
83. Liu, Q. et al. Kinome-wide selectivity profiling of ATP-competitive mammalian target of rapamycin (mTOR) inhibitors and characterization of their binding kinetics. *J. Biol. Chem.* **287**, 9742–9752 (2012).
84. Liu, Q. et al. Characterization of Torin2, an ATP-competitive inhibitor of mTOR, ATM, and ATR. *Cancer Res.* **73**, 2574–2586 (2013).
85. Montane, M. H. & Menand, B. ATP-competitive mTOR kinase inhibitors delay plant growth by triggering early differentiation of meristematic cells but no developmental patterning change. *J. Exp. Bot.* **64**, 4361–4374 (2013).
86. Pearce, L. R. et al. Characterization of PF-4708671, a novel and highly specific inhibitor of p70 ribosomal S6 kinase (S6K1). *Biochem. J.* **431**, 245–255 (2010).

Acknowledgements We thank A. von Arnim, D. Anwesha, S. H. Wu, and C. Meyer for sharing pRPS6(S237), pRPS6(S240) and RPS6 antibodies with detailed protocols; C. Meyer, J. Brunkard, C. Dean, D. Bouyer, Y. H. Cui, J. Goodrich, S. Brady, M. de Lucas and ABRC for providing *Arabidopsis* lines; H. Y. Qi for supplying the human 293T cells; J. Bush for plant management; S. Jiang and F. Marchan for help with insect cell expression system; B. Ardehali, C. Tsokos, F. K. Hsieh and C. H. Yang for sharing reagents and discussions; C. Dufresne from Thermo Scientific Training Institute for advice on LC-MS/MS analysis; X. Fang, A. Diener, L. Li, J. Bush, T. C. Chen and H. Y. Cho for critical reading of the manuscript. This work was supported by the NIH grants GM060493 and GM129093 to J. Sheen and R.Y., the Agriculture and Food Research Initiative (2020-67013-31615) from the USDA-NIFA to S. Chen, and National Natural Science Foundation of China (31770285) to Y.Z.

Author contributions R.Y. and J. Sheen conceived and initiated the project, and designed the experiments. R.Y., H.D., J. Shin, L.S., and Y.W. performed experiments. L.X. provided the GFP-FIE/fie transgenic line. K.L. developed the PUP-IT assay and provided the plasmid. M.W. and Y.Z. performed bioinformatics analyses. S. Chhajed, J.K. and S. Chen conducted phosphoprotein enrichment, LC-MS/MS data acquisition and analysis. R.Y. and J. Sheen wrote the manuscript. All authors discussed the results and commented on the manuscript.

Competing interests The authors declare no competing interests.

Additional information

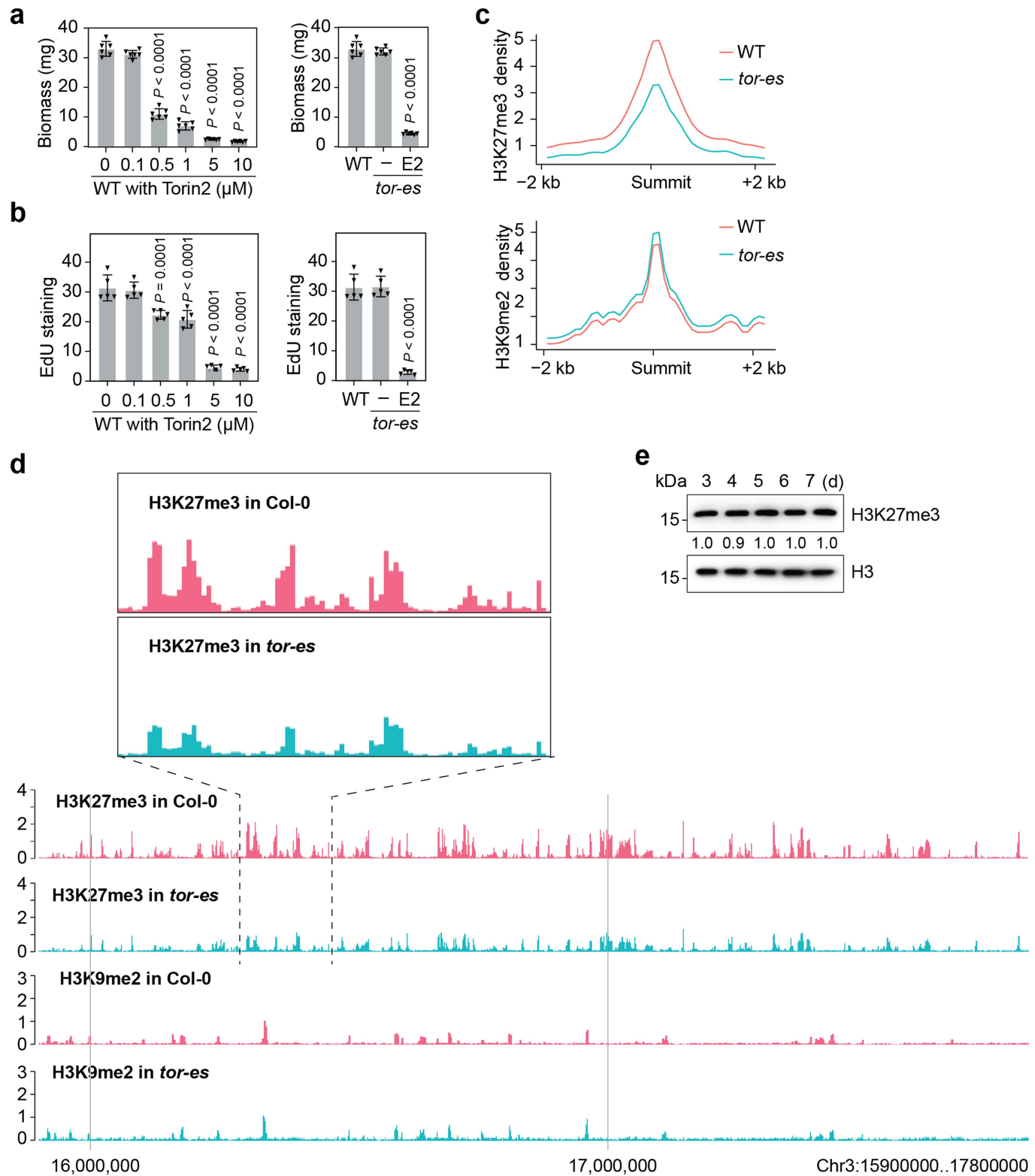
Supplementary information The online version contains supplementary material available at <https://doi.org/10.1038/s41586-022-05171-5>.

Correspondence and requests for materials should be addressed to Ruiqiang Ye or Jen Sheen.

Peer review information *Nature* thanks the anonymous reviewer(s) for their contribution to the peer review of this work. Peer reviewer reports are available.

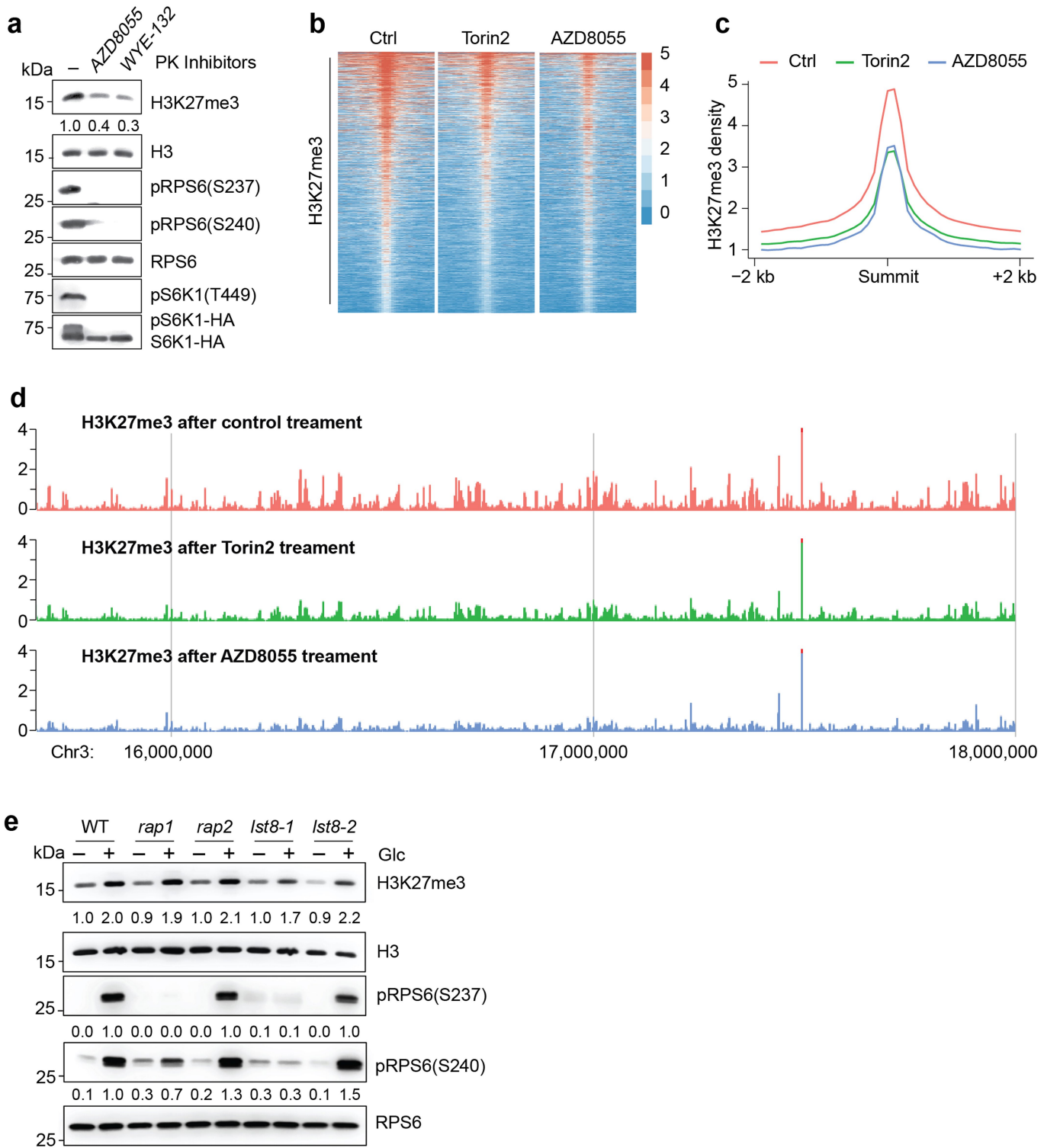
Reprints and permissions information is available at <http://www.nature.com/reprints>.

Article



Extended Data Fig. 1 | TOR controls the global H3K27me3 level and development. **a**, TOR differentially regulates seedling biomass. WT seedlings treated with different concentrations of Torin2 or *tor-es* seedlings at 8 days after germination. (n = 6 seedlings). **b**, Distinct TOR activity thresholds regulate DNA replication. Quantification of EdU staining in roots (n = 5 seedlings). **c**, Metaplots showing ChIP-Rx-seq read density. H3K27me3 and H3K9me2 in 7-day WT and *tor-es*. The ChIP-seq data are normalized with an exogenous reference genome. The peak summits ±2 kb is shown. **d**, Genome

browser view of H3K27me3 and H3K9me2 ChIP-seq read densities in WT and *tor-es*. The *Arabidopsis* genome region within Chr3:15900000..17800000 is shown. An enlarged view of a selected region is shown on the top. **e**, The H3K27me3 level in plants grown in sugar-containing medium. d, day. Values are the relative level of H3K27me3 compared with the corresponding H3 control, with immunoblot signals in day 3 set as 1.0. Experiments were conducted in three biological repeats with similar results. Data in **a, b** show mean ± s.d., one-way ANOVA with Tukey's multiple comparisons test.

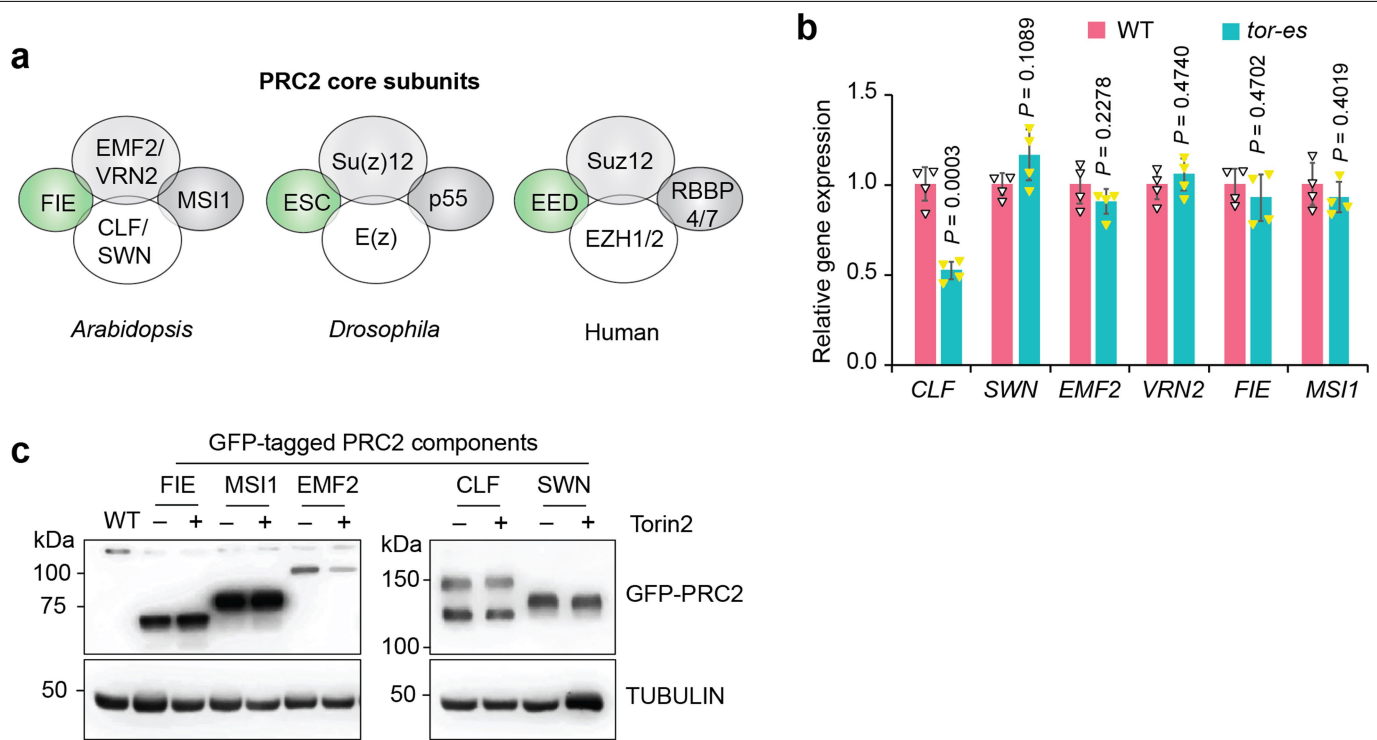


Extended Data Fig. 2 | See next page for caption.

Article

Extended Data Fig. 2 | TOR controls the global H3K27me3 level. **a-d**, TOR regulates global H3K27me3 levels. **a**, TOR but not S6K regulates global H3K27me3 levels. WT or S6K1-HA transgenic seedlings were treated with 10 µM of different inhibitors for 3 days. At 7 days, TOR activity was monitored by pS6K1(T449) and the band shift of pS6K1-HA. S6K activity was monitored by pRPS6(S237) and pRPS6(S240). The intensity of each immunoblot was quantified by ImageJ. Values are the relative level of H3K27me3 compared with the corresponding H3 control, with immunoblots in mock set as 1.0. **b**, Heatmap of H3K27me3 enrichment in plants with or without TOR inhibitor treatment. The colour scale indicates reference-adjusted RPM (RRPM) surrounding peak summit from the ChIP-Rx-seq data. **c**, Metaplots showing H3K27me3 ChIP-Rx-seq read density in plants with or without TOR inhibitor treatment. The ChIP-seq data are normalized with an exogenous reference

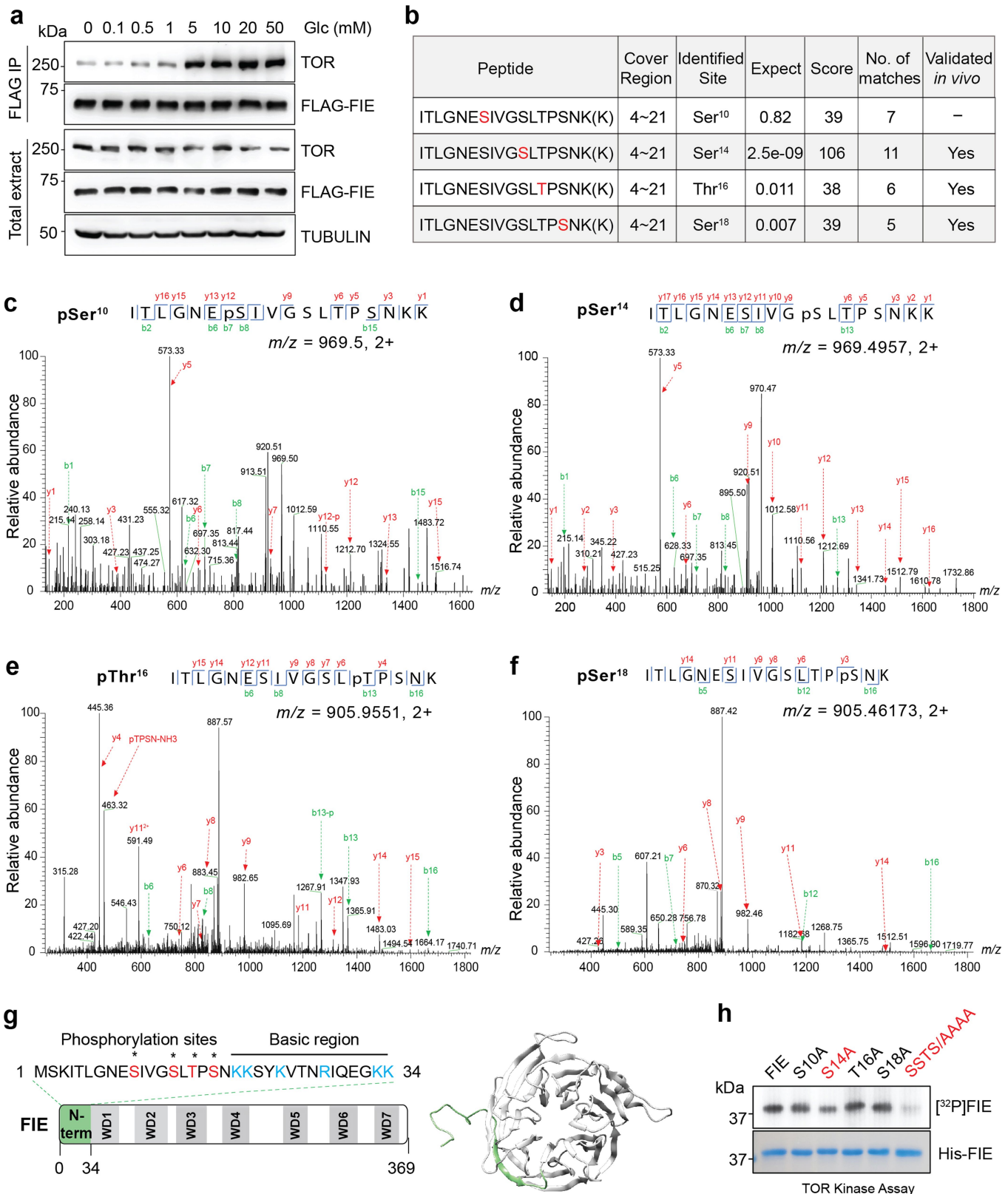
genome. The peak summits ±2 kb is shown. **d**, Genome browser view of H3K27me3 ChIP-seq read densities. The *Arabidopsis* genome region within Chr3:15800000..18000000 is shown. **e**, Differential regulation of S6K and H3K27me3 in *rpl1* and *lst8-1* mutants. The restoration of H3K27me3 was induced by 25 mM glucose for 6 h in 7-d sugar-starved seedlings. TOR-S6K activity was monitored by pRPS6(S237) and pRPS6(S240). The intensity of each immunoblot was quantified by ImageJ. Values for H3K27me3 are the relative level of H3K27me3 compared with the corresponding H3 control, with immunoblots in WT before glucose stimulation set as 1.0. Values for RPS6 phosphorylation are the relative level of pRPS6(S237) and pRPS6(S240) compared with the corresponding RPS6 control, with immunoblots in WT after glucose stimulation set as 1.0. Data in **a** and **e** are representatives of three biological replicates each.



Extended Data Fig. 3 | The transcript and protein levels of PRC2 components are not regulated by TOR. **a**, Evolutionarily conserved core PRC2 subunits in *Arabidopsis*, *Drosophila* and mammals. PRC2 components regulating plant postembryonic development are shown. **b**, RT-qPCR analysis of genes encoding PRC2 components in 7-day WT and *tor-es*. *ACT2* transcripts served as an internal control for normalization. Data show mean \pm s.d. from 4

biological replicates. Data were analysed by unpaired two-sided Student's *t* test. **c**, GFP-tagged PRC2 components are not regulated by TOR. Torin2 (10 μ M) was added for 24 h in 7-d seedlings. Tubulin was used for the loading control for the immunoblot analyses. Experiments were conducted in three biological repeats with similar results.

Article



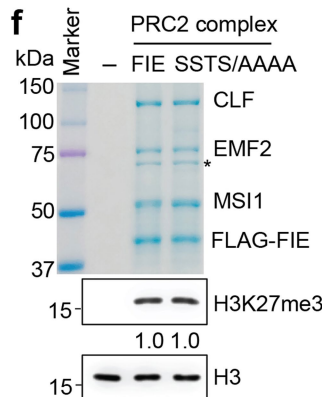
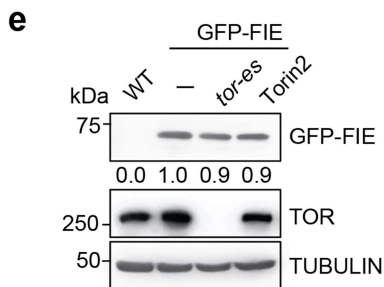
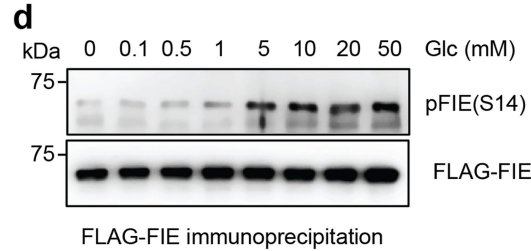
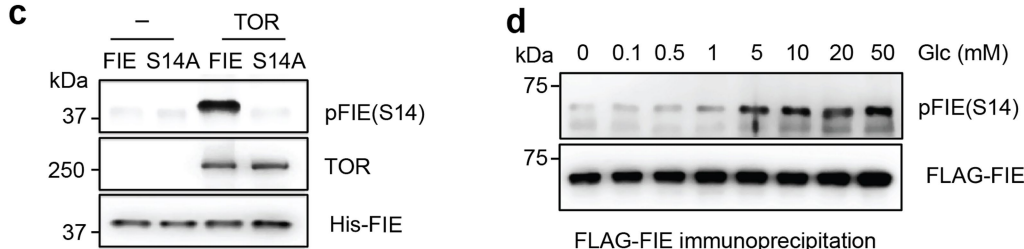
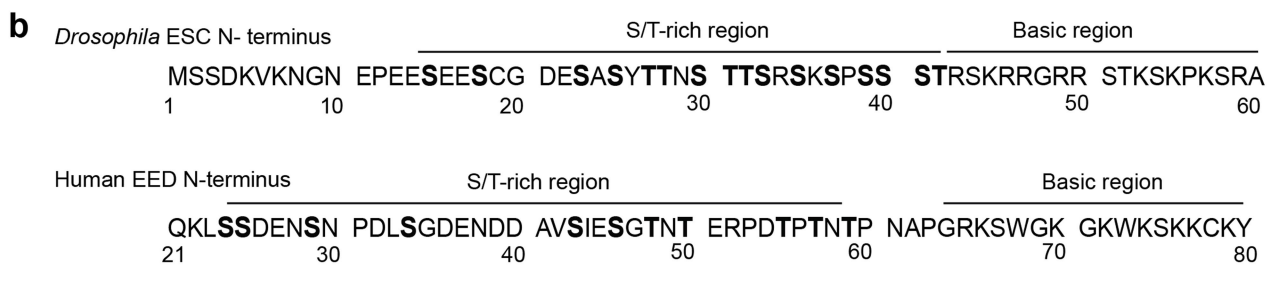
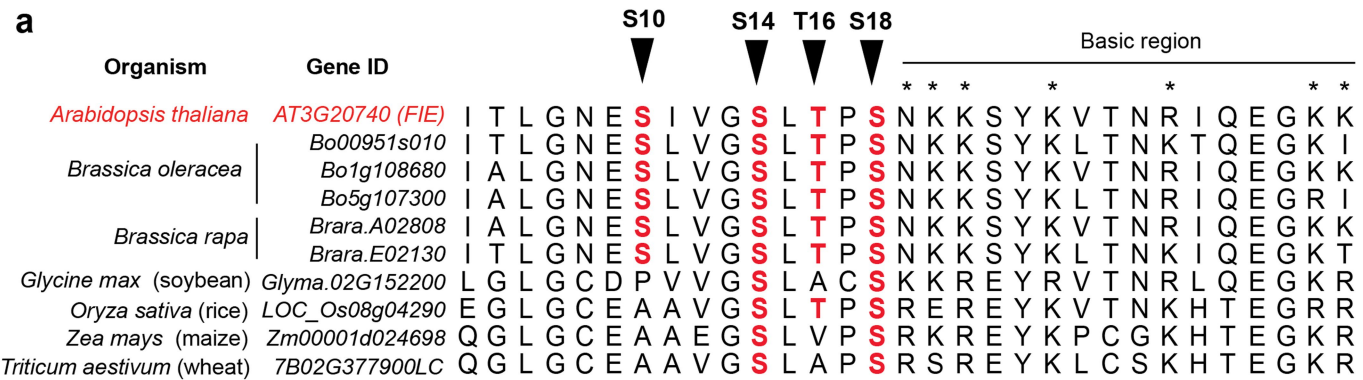
Extended Data Fig. 4 | See next page for caption.

Extended Data Fig. 4 | TOR directly interacts with and phosphorylates FIE.

a, Glucose enhances the interaction between TOR and FIE *in vivo*. Co-immunoprecipitation (Co-IP) of FLAG-tagged FIE with TOR from starved (7 d) and glucose stimulated (2 h) plants. Glc, Glucose. **b**, Summary of the TOR phosphorylation sites of FIE identified by LC-MS/MS analysis. The corresponding phosphopeptides and its covered regions are listed. Expected, the expect value indicates the probability that the peptide is matched by chance. Smaller value indicates more significance of the peptide identification. Score, the score value represents a calculation of how well the observed spectrum fits to the identified peptide. Higher value indicates higher confidence of the peptide identification. No. of matches, the total number of matched peptides with the same modifications and sites from three biological repeats. Validated *in vivo*, the modified peptides were identified from *in vivo* FLAG-FIE immunoprecipitation. **c**, Mass spectrometric analysis of pS10

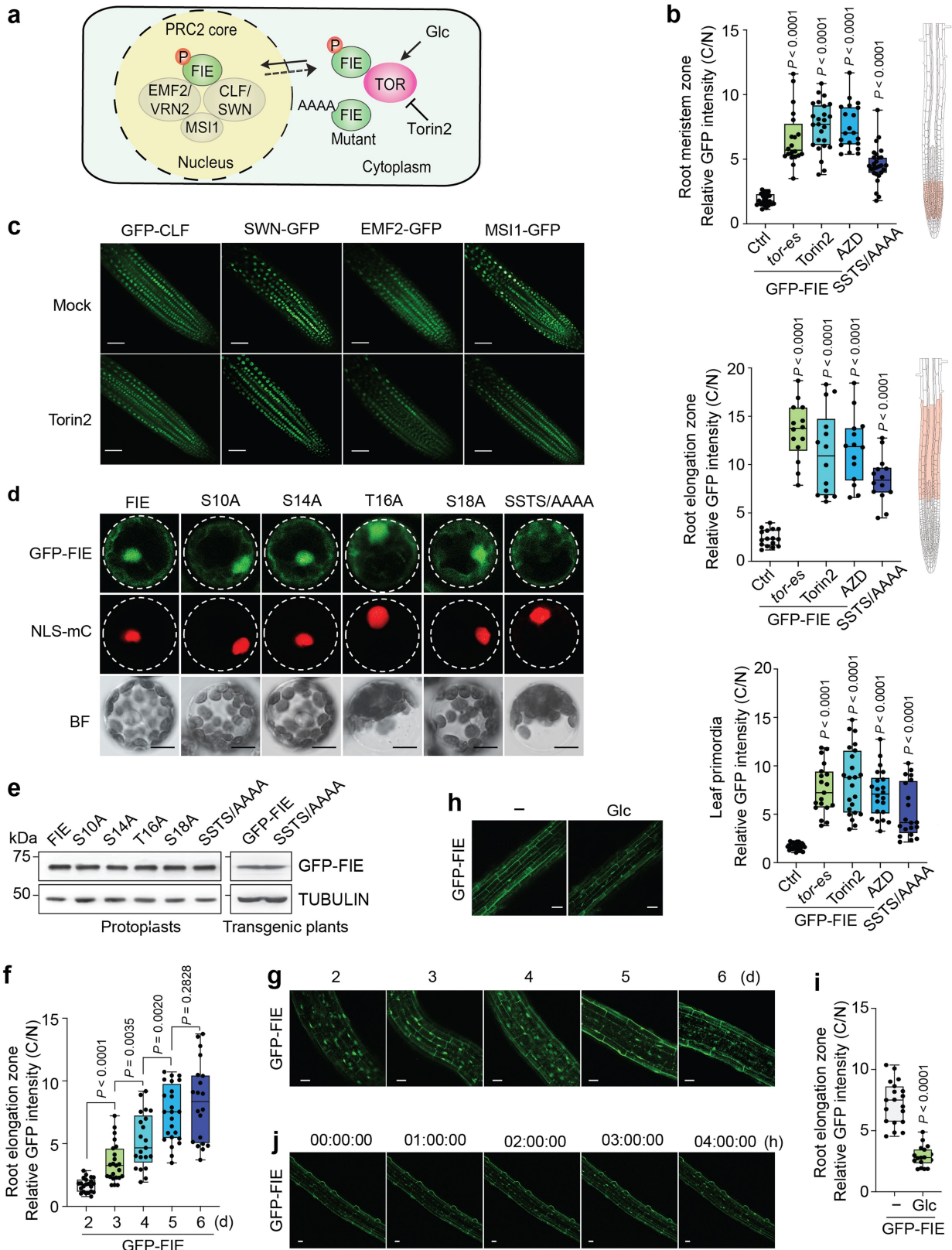
peptide from *in vitro* TOR kinase assay. **d**, Mass spectrometric analysis of pS14 peptide from *in vitro* TOR kinase assay. **e**, Mass spectrometric analysis of pT16 peptide from *in vitro* TOR kinase assay. **f**, Mass spectrometric analysis of pS18 peptide from *in vivo* FLAG-FIE immunoprecipitation. **g**, The predicted FIE structure. The N-terminal 34 aa sequence is shown with phosphorylation sites (red) identified by mass spectrometry and the basic residues (blue). The predicted 3D structure of FIE by modelling is shown with the flexible N-terminal domain highlighted in green (right). **h**, TOR phosphorylation of FIE variants by *in vitro* kinase assays. Single or quadruple mutants of FIE protein was used as the substrate. Phosphorylation of His-FIE by TOR is shown with autoradiography (top). Protein loading control is shown by Coomassie blue staining (bottom). Experiments were conducted in three biological repeats with similar results.

Article



Extended Data Fig. 5 | Conservation of the key TOR phosphorylation sites in plant FIE and animal orthologs. **a**, Phosphosite conservation was analysed by multiple sequence alignment of FIE proteins from reference organisms using PLAZA 4.0 Dicots (https://bioinformatics.psb.ugent.be/plaza/versions/plaza_v4_dicots/). The selection of reference organisms includes *Arabidopsis*, *Brassica*, soybean, rice, maize and wheat. The four arrow heads indicate the potential phosphorylation residues. **b**, N-terminal sequences of *Drosophila* ESC (residues 1–60) and human EED (residues 21–80) are shown. Highly conserved positions of S/T-rich and basic regions are indicated. **c**, Immunoblot validation of pFIE(S14) specific antibody using the *in vitro* TOR-FIE kinase assay. **d**, Glucose enhances pFIE(S14) levels. Immunoblot analysis of pFIE(S14) after IP with

anti-FLAG in starved (7 d) transgenic FLAG-GFP-FIE seedlings and stimulated by different concentrations of glucose for 2 h. **e**, GFP-FIE protein levels are not regulated in *tor-es* or Torin2 treated 7-d seedlings. A specific TOR antibody was used to detect endogenous TOR by immunoblot analysis. Tubulin served as the loading control. Values are the relative level of GFP-FIE over Tubulin, with blots in mock treatment set as 1.0. **f**, *In vitro* histone methyltransferase assays using H3 substrate and recombinant *Arabidopsis* PRC2 complexes from insect Sf9 cells. The complexes stained by Coomassie blue were purified with FLAG-tagged WT or the mutant form (SSTS/AAAA) of FIE. The H3K27me3 was detected by immunoblot and quantified by comparing to the corresponding H3 control.



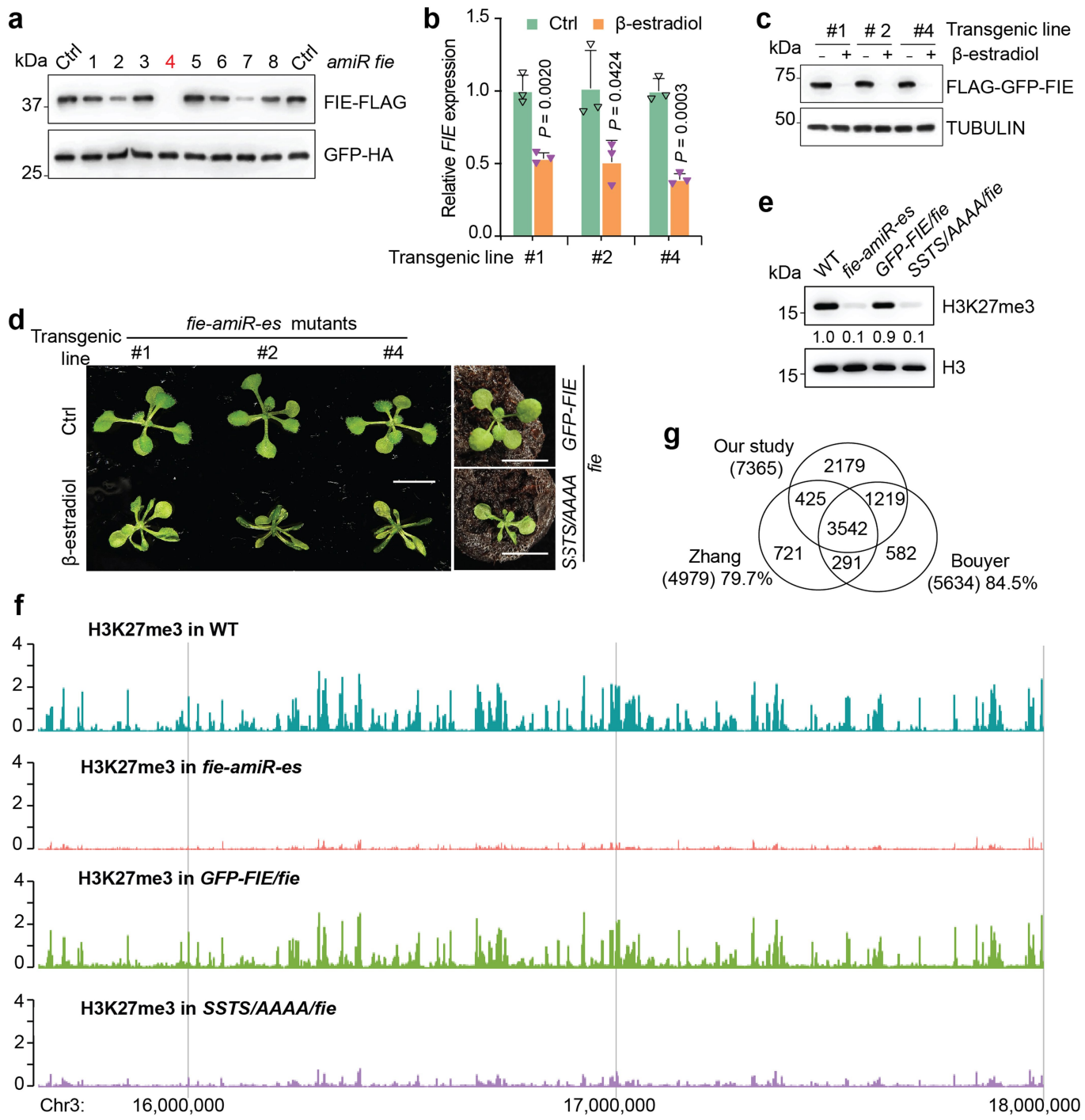
Extended Data Fig. 6 | See next page for caption.

Article

Extended Data Fig. 6 | Glucose-TOR specifically promotes the cytoplasm-to-nucleus translocation of FIE to enhance the PRC2 activity in the nucleus.

a, A proposed model for the cytoplasm-to-nucleus translocation of FIE regulated by TOR. FIE mainly localizes in the cytoplasm at low TOR activity and its phosphorylation by glucose-activated TOR stimulates its nuclear entry to enhance PRC2 activity. Blocking TOR activity or mutation of the phosphorylation sites inhibited the nuclear translocation of FIE. **b**, Quantitative confocal imaging of GFP-FIE and GFP-FIE(SSTS/AAAA) in leaf primordia and roots. The cytoplasm/nucleus (C/N) signal intensity ratio of GFP-FIE or GFP-FIE(SSTS/AAAA) at the single-cell level was measured by quantitative confocal imaging using the Leica LAS-X software. WT seedlings (5 d) expressing GFP-FIE without (Ctrl) or with 10 μ M of Torin2 or AZD treatment (24 h) or *tor-es* (10 μ M estradiol for 3 d) were examined. Root elongation zone and root meristem zone are illustrated. **c**, Confocal images of GFP-tagged PRC2 components in the meristem zone of roots. Plants were imaged with or without (Mock) Torin2 treatment. **d**, Confocal images of GFP-tagged FIE and mutants in protoplasts. BF, bright field. NLS-mC denotes nuclear HY5-mCherry as a control for protoplasts co-transfection and nuclear localization. Scale bars, 10 μ m. Images are representative of 10 protoplasts

from three biological repeats. **e**, Immunoblot analysis of GFP-tagged FIE variants expressed in protoplast and transgenic plants. Tubulin was used for the loading control. Data are representatives of three biological replicates. **f,g**, The dynamics of GFP-FIE during glucose starvation. **f**, Confocal images of GFP-FIE from 2–6 d in the root elongation zone in glucose-free medium. **g**, Quantitative confocal imaging of GFP-FIE C/N ratio. **h,i,j**, Glucose stimulates dynamic nuclear translocation of GFP-FIE after starvation in the root elongation zones. **h**, Confocal images of GFP-FIE without or with 25 mM glucose stimulation for 6 h in starved seedlings (5 d). **i**, Quantitative confocal imaging of GFP-FIE C/N ratio. **j**, Time-lapse live imaging of glucose stimulated nuclear translocation of GFP-FIE in the root elongation zone. Representative images were taken from Supplementary Video at 1–4 h time points after 25 mM glucose stimulation. The experiment was repeated three times with similar results. **b,f,i**, In the boxplots, data were analysed from more than 15 cells from three experiments, and are expressed as mean \pm s.d. Centre line, median; box limits, 25th and 75th percentiles; the whiskers indicate data's minimum and maximum; the points represent each individual value. Statistical significance was determined by unpaired two-sided Student's *t* test. **c,g,h,j**, Images are representative of six seedlings from three biological repeats. Scale bar, 25 μ m.

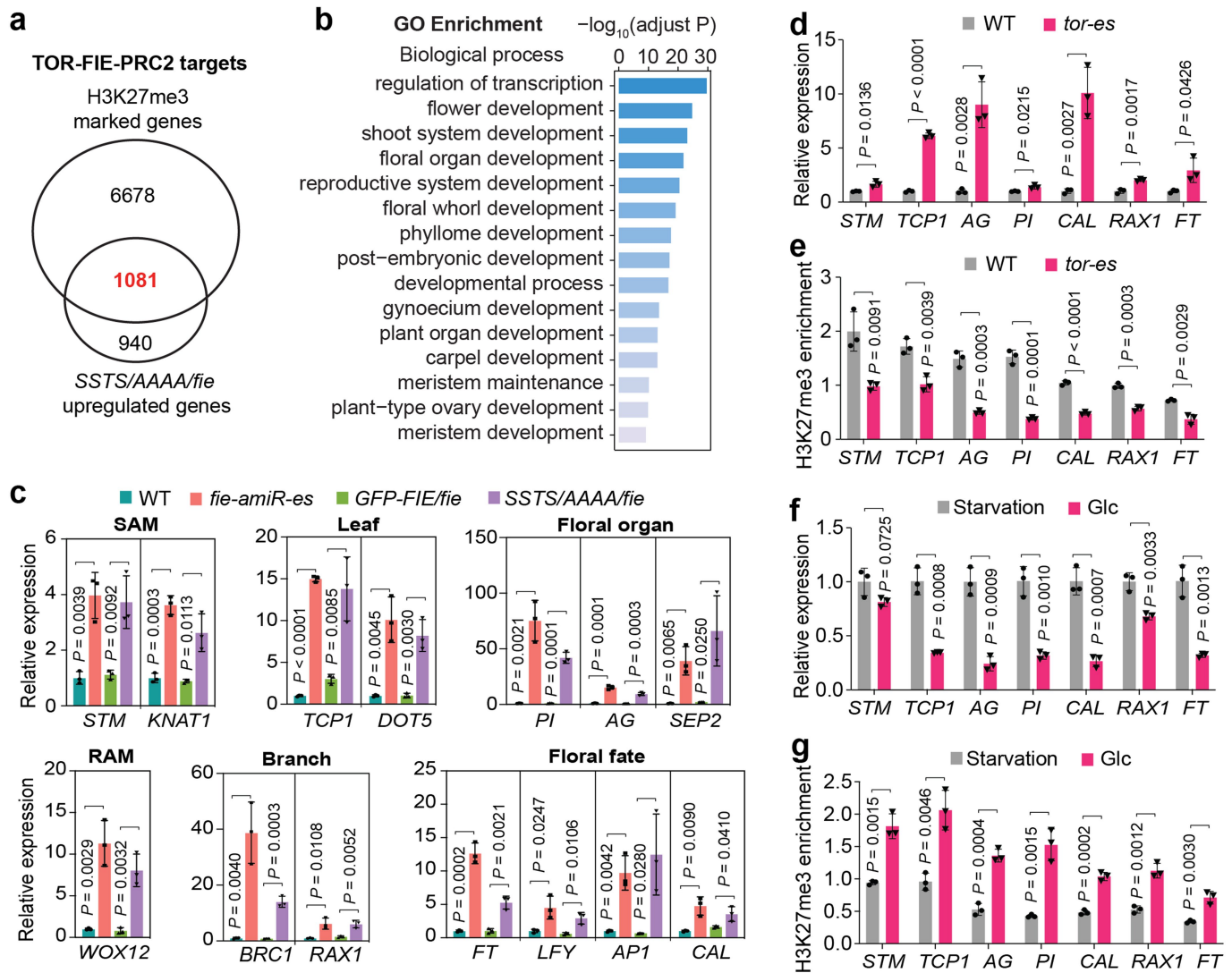


Extended Data Fig. 7 | Generation and characterization of

estradiol-inducible *fie-amiR-es* and *SSTS/AAAA/fie* mutants. **a**, Screening of optimal amiRNA in the protoplast system. Empty amiRNA expression vector as a control (Ctrl) or each of the eight amiRNA candidate plasmids was co-transfected with a heat shock promoter-driven FIE-FLAG plasmid. The HBT-GFP-HA plasmid serves as an internal control for all co-transfection experiments. Immunoblot analysis indicated similar GFP-HA protein levels. The most potent amiRNA4 abolished FIE-FLAG expression and was chosen to generate estradiol-inducible *fie-amiR-es* transgenic plants. **b**, RT-qPCR analysis of *FIE* transcripts in 14-day transgenic *fie-amiR-es* lines without or with 10 μM of estradiol treatment. *UBQ10* transcripts served as an internal control for normalization. Data show mean ± s.d. from 3 biological replicates. **c**, Protein blot analysis of FIE protein levels in 14-day transgenic *fie-amiR-es* lines. Three independent *fie-amiR-es* lines were crossed to the FLAG-GFP-FIE transgenic plant. The

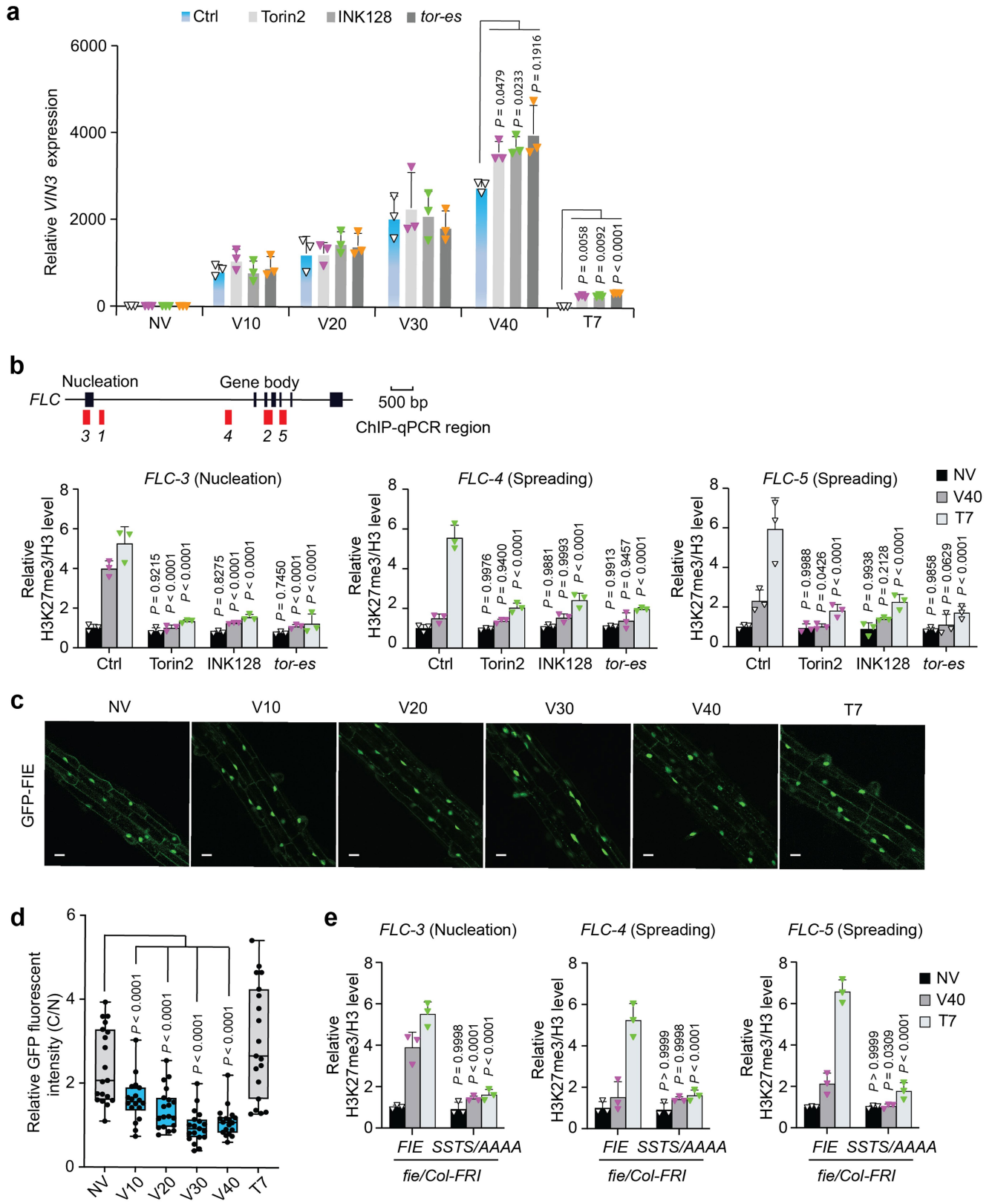
FLAG-GFP-FIE protein was eliminated with 10 μM of estradiol treatment. Tubulin was used for the loading control. **d**, The development phenotype of the *fie-amiR-es* lines was similar to that of the *SSTS/AAAA/fie* mutant. Three independent *fie-amiR-es* lines and the *SSTS/AAAA/fie* mutant showed small, narrow and curled leaves. The *GFP-FIE/fie* plant showed normal development. Scale bar, 10 mm. Experiments were conducted in three biological repeats with similar results. **e**, The H3K27me3 level was greatly decreased in 14-day *fie* mutant plants. Values are the relative level of H3K27me3 compared with the corresponding H3 control, with immunoblot signals in WT set as 1.0. **f**, Genome browser view of H3K27me3 ChIP-seq read densities. The *Arabidopsis* genome region within Chr3:15800000..18000000 is shown. **g**, Venn diagram of H3K27me3 target genes in *Arabidopsis* from three independent genome wide analyses. The H3K27me3 targets in our study cover 79.7% of genes from Zhang *et al.* and 84.5% of genes from Bouyer *et al.*¹². Data in **a**, **c**, and **e** are representatives of three biological replicates each.

Article



Extended Data Fig. 8 | The TOR-FIE-PRC2-TR relay plays a central role in diverse developmental programs. **a**, TOR-FIE-PRC2 target genes. These genes are marked by H3K27me3 and upregulated in the *SSTS/AAAAA/fie* mutant. **b**, Gene Ontology enrichment analysis of TOR-FIE-PRC2 target genes in biological process terms related to transcriptional regulation and development. Fisher's exact test was used by the BiNGO to identify GO terms that are significantly over-represented with the compiled gene list. FDR, false discovery rate. The categories in biological process with fold enrichment > 2 and FDR < 10⁻¹⁰ were selected and presented. **c**, PRC2 target genes are transcription regulators upregulated in *fie* mutants (14d). *UBQ10* or *ACT2*

transcripts served as an internal control for normalization. **d-f**, RT-qPCR analysis of TOR-FIE-PRC2 target genes in WT and *tor-es*. **(d)** In sugar-containing medium or (**f**) in sugar-free medium and without or with 25 mM glucose stimulation for 6 h after starvation (7 d). *UBC21* transcripts served as an internal control for normalization. **e-g**, ChIP-qPCR analysis of H3K27me3 enrichment on TOR-FIE-PRC2 target genes in 7-day WT and *tor-es*. **(e)** in sugar-containing medium or (**g**) in sugar-free medium and without and with 25 mM glucose stimulation for 6 h after starvation (7 d). ChIP-qPCR data were normalized to percentage of input DNA. **c-g**, Data show mean ± s.d. from 3 biological replicates. Data were analysed by unpaired two-sided Student's *t* test.

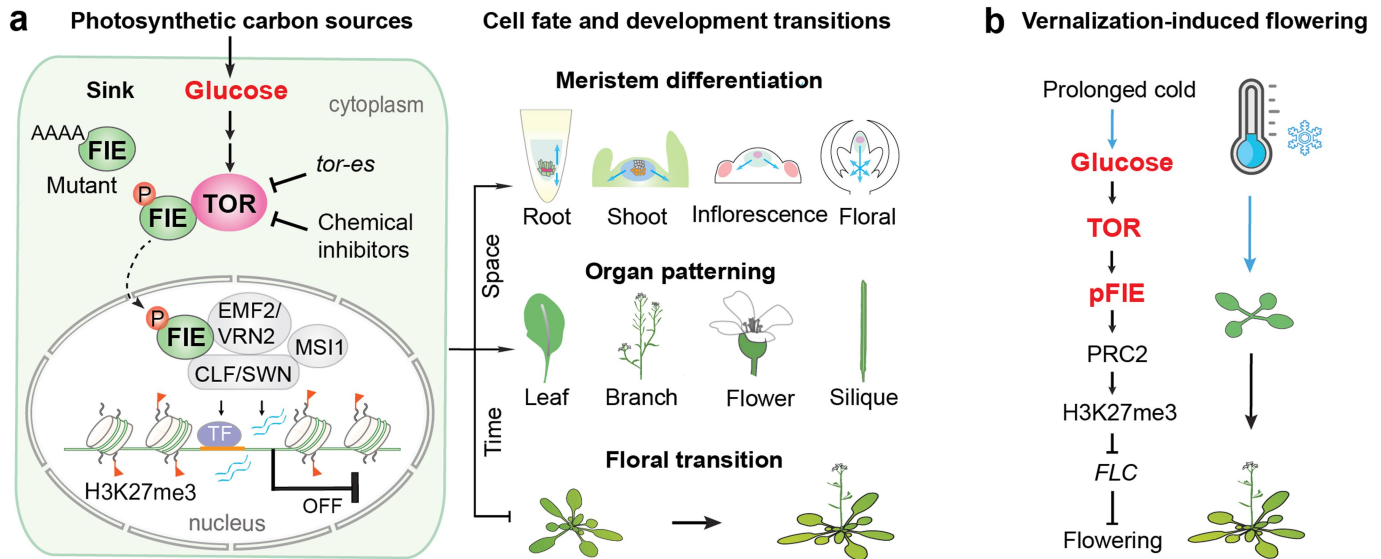


Extended Data Fig. 9 | See next page for caption.

Article

Extended Data Fig. 9 | *VIN3* expression, H3K27me3 enrichment at *FLC*, and GFP-FIE nuclear translocation during vernalization. **a**, *VIN3* induction by vernalization is not regulated by TOR. Seedlings were treated at 4 °C to induce vernalization for the indicated days without (Ctrl) or with TOR inhibitors (1 μM Torin2 and INK128), or in the inducible *tor-es* mutant. Data are relative to the *UBC21* (*At5g25760*) expression as a control gene and normalized to non-vernalized (NV) levels of ctrl plants. Data show mean ± s.d. from 3 biological replicates, two-way ANOVA with Tukey's multiple comparisons test. **b**, TOR deficiency reduces H3K27me3 levels at *FLC*. Relative H3K27me3/H3 level normalized to that of ctrl plants under non-vernalized (NV) condition as 1. Black boxes, exons. Red boxes, selected regions for H3K27me3 ChIP-qPCR analyses. bp, base pairs. *FLC-3* and *FLC-4,5* are located in the nucleation and spreading regions of H3K27me3 at *FLC*, respectively. **c, d**, Prolonged cold treatment prompts the nuclear localization of GFP-FIE in the elongation zones of roots. **c**, Confocal images of GFP-FIE during vernalization. Images are

representative of six seedlings from three biological repeats. Scale bar, 25 μm. **d**, Quantitative confocal imaging of GFP-FIE in the root elongation zone. The cytoplasm/nucleus (C/N) signal intensity ratio of GFP-FIE at the single-cell level was measured by quantitative confocal imaging using the Leica LAS-X software. In the boxplot, data were analysed from more than 15 cells from three experiments, and are expressed as mean ± s.d. Centre line, median; box limits, 25th and 75th percentiles; the whiskers indicate data's minimum and maximum; the points represent each individual value. Statistical significance was determined by unpaired two-sided Student's *t* test. **e**, Vernalization induced H3K27me3 levels at *FLC* are compromised in *AAAA/fie-FRI*. Relative H3K27me3/H3 level was normalized to that of *fie/Col-FRI* plants under non-vernalized (NV) condition as 1. Data in **b, e** show mean ± s.d. from 3 biological replicates, two-way ANOVA with Tukey's multiple comparisons test; NV, non-vernalized. V, vernalization days at 4 °C. T, postcold days at 22 °C.



Extended Data Fig. 10 | Model of the Glucose-TOR-FIE-PRC2 signalling network governing diverse developmental programs. a, The Glucose-TOR-FIE-PRC2 signalling network. Optimal photosynthesis in source leaves produces sugars that are transported to energy demanding sinks, including apical and lateral meristems, developing leaf primordia and young leaves, roots, flowers, fruits and seeds, to support their growth and development. In the sink, glucose derived from local or systemic carbon sources is metabolized to activate TOR kinase, which interacts with and phosphorylates FIE in the cytoplasm. The phosphorylated FIE is translocated into the nucleus to enhance PRC2 activity, which are recruited to the specific chromatin loci by

transcription factors (TF), cis-regulatory elements (orange bar), and noncoding RNAs (blue waving lines) to deposit H3K27me3 and silence master transcription regulators controlling diverse developmental programs. This molecular mechanism orchestrates plant developmental fates, organogenesis, patterning and provides a direct and global mechanistic connection between glucose-TOR signalling and development. **b,** The Glucose-TOR-FIE-PRC2-FLC relay overrides the default vegetative developmental program to promote flowering. This molecular mechanism may underly the link between glucose and vernalization-mediated floral transition stimulated by prolonged cold exposure.

Corresponding author(s): Jen Sheen

Last updated by author(s): Jun 24, 2022

Reporting Summary

Nature Portfolio wishes to improve the reproducibility of the work that we publish. This form provides structure for consistency and transparency in reporting. For further information on Nature Portfolio policies, see our [Editorial Policies](#) and the [Editorial Policy Checklist](#).

Statistics

For all statistical analyses, confirm that the following items are present in the figure legend, table legend, main text, or Methods section.

n/a Confirmed

- The exact sample size (n) for each experimental group/condition, given as a discrete number and unit of measurement
- A statement on whether measurements were taken from distinct samples or whether the same sample was measured repeatedly
- The statistical test(s) used AND whether they are one- or two-sided
Only common tests should be described solely by name; describe more complex techniques in the Methods section.
- A description of all covariates tested
- A description of any assumptions or corrections, such as tests of normality and adjustment for multiple comparisons
- A full description of the statistical parameters including central tendency (e.g. means) or other basic estimates (e.g. regression coefficient) AND variation (e.g. standard deviation) or associated estimates of uncertainty (e.g. confidence intervals)
- For null hypothesis testing, the test statistic (e.g. F , t , r) with confidence intervals, effect sizes, degrees of freedom and P value noted
Give P values as exact values whenever suitable.
- For Bayesian analysis, information on the choice of priors and Markov chain Monte Carlo settings
- For hierarchical and complex designs, identification of the appropriate level for tests and full reporting of outcomes
- Estimates of effect sizes (e.g. Cohen's d , Pearson's r), indicating how they were calculated

Our web collection on [statistics for biologists](#) contains articles on many of the points above.

Software and code

Policy information about [availability of computer code](#)

Data collection

For LC-MS/MS analysis, the Orbitrap Fusion Tribrid mass spectrometer (Thermo Scientific) was used to collect data. Confocal images were acquired using the Leica Application Suite X software on a Leica TCS SP8 (Leica) confocal microscope. For genome-wide analysis, the libraries were sequenced using an Illumina HiSeq4000 at GENEWIZ Next Generation Sequencing centre.

Data analysis

The raw data of LC-MS/MS spectra was analysed by the Mascot search engine (version 2.2, Matrix Science). For the confocal images of leaf primordia, The autofluorescence signal was removed by applying the Channel and Spectral Dye Separation tool (Leica). The images were further processed using Adobe Photoshop (version 21.1.0) or ImageJ (version 2.3.0/1.53q). Quantification of subcellular localization of GFP-FIE were performed using LAS X (Leica Application Suite v. X3.1.1.15751) For RNA-seq analysis, sequenced reads were mapped to the Arabidopsis (TAIR10) genome with HISAT273 program (version 2.1.0). The featureCount program of Subread74 package (version 1.5.3) was used to quantify the RNA-seq expression levels of the TAIR10 annotated gene models. DEseq275 was used to determine the significance of the differential expression between samples with the combined criteria: $|\log_{2}\text{foldchange}| \geq 1$ and $\text{FDR} \leq 0.05$. For ChIP-Seq analysis, sequencing adaptors were removed using Trimmomatic (version 0.36); the ChIP-seq reads were mapped to Arabidopsis (TAIR10) and human (hg19) combined genomes, using BWA-MEM (version 0.7.15-r1142-dirty). MACS2 utility callpeak was used to identify read-enriched regions (peaks) and utility pileup was used to generate bedgraph files with default settings. The bedGraphToBigWig (version 4) of UCSC was used to transfer bedgraph files to bigwig files, and then the bigwig files were loaded onto JBrowse74 (version 1.12.1) for data visualization.
No custom codes were central to the conclusions of the paper.

For manuscripts utilizing custom algorithms or software that are central to the research but not yet described in published literature, software must be made available to editors and reviewers. We strongly encourage code deposition in a community repository (e.g. GitHub). See the Nature Portfolio [guidelines for submitting code & software](#) for further information.

Data

Policy information about [availability of data](#)

All manuscripts must include a [data availability statement](#). This statement should provide the following information, where applicable:

- Accession codes, unique identifiers, or web links for publicly available datasets
- A description of any restrictions on data availability
- For clinical datasets or third party data, please ensure that the statement adheres to our [policy](#)

Sequencing data are deposited to the Gene Expression Omnibus (accession no. GSE161807). All other data of this manuscript are presented in the main text or in the supplementary materials (uncropped blots and gel images, primers, and source data behind all graphs). The sequences of Arabidopsis genome (TAIR10), DNA and proteins were obtained from TAIR (<https://www.arabidopsis.org/>) and NCBI (<https://www.ncbi.nlm.nih.gov/>). The 3D protein structures were predicted by RaptorX (<http://raptordx.uchicago.edu/>). The pCambia-PUP-IT vector was deposited to Addgene (#186478). The plasmids and the transgenic Arabidopsis seeds generated in this study are available upon request.

Field-specific reporting

Please select the one below that is the best fit for your research. If you are not sure, read the appropriate sections before making your selection.

Life sciences Behavioural & social sciences Ecological, evolutionary & environmental sciences

For a reference copy of the document with all sections, see nature.com/documents/nr-reporting-summary-flat.pdf

Life sciences study design

All studies must disclose on these points even when the disclosure is negative.

Sample size	Sample sizes were chosen to make sure that the observed effects are significant by statistical analysis, as well as consideration of previous publications on similar experiments. All the experiments were performed on at least three biological samples. For flowering time assay during vernalization, refer to Jiang and Berger, Science 357, 1146, 2017.
Data exclusions	No data were excluded from the analysis.
Replication	All the experiments in this study were repeated at least 3 times with consistent results. For phenotype analysis, at least 10 independent plants were analysed.
Randomization	Multiple transgenic plants of different constructs were randomly selected with no formal randomization techniques to minimize the position effect on the genome. And plant samples were also randomly selected from a large pool grown in identical conditions for protein or RNA analysis.
Blinding	For RNA-seq, ChIP-seq, and LC-MS/MS analysis in the study, sample preparation, data acquisition, and analysis were performed with the collaboration of authors from different labs without prior knowledge of results. For all the others, since the author who performed the experiment also analysed the data, blind was not applied.

Reporting for specific materials, systems and methods

We require information from authors about some types of materials, experimental systems and methods used in many studies. Here, indicate whether each material, system or method listed is relevant to your study. If you are not sure if a list item applies to your research, read the appropriate section before selecting a response.

Materials & experimental systems

n/a	Involved in the study
<input type="checkbox"/>	<input checked="" type="checkbox"/> Antibodies
<input checked="" type="checkbox"/>	<input type="checkbox"/> Eukaryotic cell lines
<input checked="" type="checkbox"/>	<input type="checkbox"/> Palaeontology and archaeology
<input checked="" type="checkbox"/>	<input type="checkbox"/> Animals and other organisms
<input checked="" type="checkbox"/>	<input type="checkbox"/> Human research participants
<input checked="" type="checkbox"/>	<input type="checkbox"/> Clinical data
<input checked="" type="checkbox"/>	<input type="checkbox"/> Dual use research of concern

Methods

n/a	Involved in the study
<input type="checkbox"/>	<input checked="" type="checkbox"/> ChIP-seq
<input checked="" type="checkbox"/>	<input type="checkbox"/> Flow cytometry
<input checked="" type="checkbox"/>	<input type="checkbox"/> MRI-based neuroimaging

Antibodies

Antibodies used

Rabbit anti-Histone H3 antibody, Abcam, Cat# ab1791;

Antibodies used	Rabbit anti-Histone H3K4me3 Antibody, Abcam, Cat# ab8580; Mouse anti-Histone H3K9me2 antibody, Abcam, Cat# ab1220; Rabbit anti-Histone H3K27me3 Antibody, Sigma-Aldrich, Cat# 07-449; Rabbit anti-Histone H3K36me3 Antibody, Abcam, Cat# ab9050; Rabbit anti-TOR antibody; homemade Rabbit anti-pS6K1(T449) antibody; homemade Rabbit anti-pFIE(S14) antibody; home-made Rabbit anti-RPS6 antibody; requested from S.H. Wu's lab Rabbit anti-pRPS6(S237) antibody; requested from A. von Arnim's lab Rabbit anti-pRPS6(S240) antibody; requested from A. von Arnim's lab Mouse anti-GFP antibody, CLONTECH, Cat# 632381; Mouse monoclonal anti-Tubulin [B-5-1-2], SIGMA-Aldrich, Cat# T5168; Rat anti-HA-Peroxidase antibody, SIGMA-Aldrich, Cat# 12013819001; Mouse anti-FLAG M2-Peroxidase antibody, SIGMA-Aldrich, Cat# A8592; Mouse anti-C-MYC-Peroxidase antibody, Roche, Cat# 1-814-150; Goat polyclonal anti-Mouse IgG-HRP, SIGMA-Aldrich, Cat# A4416; Goat polyclonal anti-Rabbit IgG-HRP, SIGMA-Aldrich, Cat# A0545.
Validation	Rabbit anti-Histone H3 antibody, 1:5000 dilution for immunoblot and 1:1000 dilution for ChIP, validation refers to "Abcam Cat# ab1791, RRID: AB_302613" and " https://www.abcam.com/Histone-H3-antibody-Nuclear-Marker-and-ChIP-Grade-ab1791.html "; Rabbit anti-Histone H3K4me3 Antibody, 1:1000 dilution for immunoblot, validation refers to "Cat# ab8580; RRID: AB_306649" and " https://www.abcam.com/histone-h3-tri-methyl-k4-antibody-chip-grade-ab8580.html "; Mouse anti-Histone H3K9me2 antibody, 1:1000 dilution for immunoblot and 1:200 dilution for ChIP, validation refers to "Cat# ab1220; RRID: AB_449854" and " https://www.abcam.com/histone-h3-di-methyl-k9-antibody-mabcam-1220-chip-grade-ab1220.html "; Rabbit anti-Histone H3K27me3 Antibody, 1:1000 dilution for immunoblot and 1:200 dilution for ChIP, validation refers to "Cat# 07-449; RRID: AB_310624" and " https://www.emdmillipore.com/US/en/product/Anti-trimethyl-Histone-H3-Lys27-Antibody-MM_NF-07-449 "; Rabbit anti-Histone H3K36me3 Antibody, Abcam, 1:1000 dilution for immunoblot, validation refers to "Cat# ab9050; RRID: AB_306966" and " https://www.abcam.com/histone-h3-tri-methyl-k36-antibody-chip-grade-ab9050.html "; Rabbit anti-TOR antibody, 1:1000 dilution for immunoblot, was used according to "Xiong and Sheen, J Biol Chem 287, 2836-2842, doi:10.1074/jbc.M111.300749 (2012)"; Rabbit anti-pS6K1(T449) antibody, 1:500 dilution for immunoblot, was used according to "Xiong and Sheen, J Biol Chem 287, 2836-2842, doi:10.1074/jbc.M111.300749 (2012)"; Rabbit anti-pFIE(S14) antibody, 1:500 dilution for immunoblot, validated in this study; Rabbit anti-RPS6 antibody, 1:5000 dilution for immunoblot, was used according to "Chen et al., Proc Natl Acad Sci U S A 115, 12823-12828, doi:10.1073/pnas.1809526115 (2018)"; Rabbit anti-pRPS6(S237) antibody, 1:3000 dilution for immunoblot, was used according to "Enganti, R. et al., Front Plant Sci 8, 2210, doi:10.3389/fpls.2017.02210 (2017)"; Rabbit anti-pRPS6(S240) antibody, 1:3000 dilution for immunoblot, was used according to "Enganti, R. et al., Front Plant Sci 8, 2210, doi:10.3389/fpls.2017.02210 (2017)"; Mouse anti-GFP antibody, 1:5000 dilution for immunoblot, validation refers to "Cat# 632381; RRID: AB_2313808" and " https://www.takarabio.com/products/antibodies-and-elisa/fluorescent-protein-antibodies/green-fluorescent-protein-antibodies "; Mouse monoclonal anti-Tubulin [B-5-1-2], 1:5000 dilution for immunoblot, validation refers to "Cat# T5168; RRID: AB_477579" and " https://www.sigmal Aldrich.com/US/en/product/sigma/t5168 "; Rat anti-HA-Peroxidase antibody, 1:5000 dilution for immunoblot, validation refers to "Cat# 12013819001; RRID: AB_390917" and " https://www.sigmal Aldrich.com/US/en/product/roche/12013819001 "; Mouse anti-FLAG M2-Peroxidase antibody, 1:5000 dilution for immunoblot, validation refers to "Cat# A8592; RRID: AB_439702" and " https://www.sigmal Aldrich.com/US/en/product/SIGMA/A8592 "; Mouse anti-C-MYC-Peroxidase antibody, 1:1000 dilution for immunoblot, validation refers to "Cat# 1-814-150; RRID: AB_390910" and " https://www.sigmal Aldrich.com/catalog/product/roche/11814150001?lang=en&region=US ". Goat polyclonal anti-Mouse IgG-HRP, SIGMA-Aldrich, Cat# A4416; 1:5000 dilution for immunoblot, validation refers to " https://www.sigmal Aldrich.com/US/en/product/sigma/a4416 " Goat polyclonal anti-Rabbit IgG-HRP, SIGMA-Aldrich, Cat# A0545. 1:5000 dilution for immunoblot, validation refers to " https://www.sigmal Aldrich.com/US/en/product/sigma/a0545 "

ChIP-seq

Data deposition

- Confirm that both raw and final processed data have been deposited in a public database such as [GEO](#).
 Confirm that you have deposited or provided access to graph files (e.g. BED files) for the called peaks.

Data access links

May remain private before publication.

Sequencing data for MCC has been submitted to the NCBI Gene Expression Omnibus (accession no. GSE161807).

Files in database submission

GSM4914851	amiR-fie-es_rep1	RNA-seq
GSM4914852	amiR-fie-es_rep2	RNA-seq
GSM4914853	amiR-fie-es_rep3	RNA-seq
GSM4914854	Ctrl_rep1	RNA-seq
GSM4914855	Ctrl_rep2	RNA-seq
GSM4914856	Ctrl_rep3	RNA-seq
GSM4914857	GFP-FIE_rep1	RNA-seq

GSM4914858	GFP-FIE_rep2	RNA-seq
GSM4914859	GFP-FIE_rep3	RNA-seq
GSM4914860	SSTS/AAAA_rep1	RNA-seq
GSM4914861	SSTS/AAAA_rep2	RNA-seq
GSM4914862	SSTS/AAAA_rep3	RNA-seq
GSM4914863	amiR-fie-es_H3K27me3_rep1	ChIP-seq
GSM4914864	amiR-fie-es_H3K27me3_rep2	ChIP-seq
GSM4914865	amiR-fie-es_H3K27me3_rep3	ChIP-seq
GSM4914866	Ctrl_H3K27me3_rep1	ChIP-seq
GSM4914867	Ctrl_H3K27me3_rep2	ChIP-seq
GSM4914868	Ctrl_H3K27me3_rep3	ChIP-seq
GSM4914869	GFP-FIE_H3K27me3_rep1	ChIP-seq
GSM4914870	GFP-FIE_H3K27me3_rep2	ChIP-seq
GSM4914871	GFP-FIE_H3K27me3_rep3	ChIP-seq
GSM4914872	SSTS/AAAA_H3K27me3_rep1	ChIP-seq
GSM4914873	SSTS/AAAA_H3K27me3_rep2	ChIP-seq
GSM4914874	SSTS/AAAA_H3K27me3_rep3	ChIP-seq
GSM4914875	Col-0_H3K27me3_rep1	ChIP-seq
GSM4914876	Col-0_H3K27me3_rep2	ChIP-seq
GSM4914877	Col-0_H3K27me3_rep3	ChIP-seq
GSM4914878	tor-es_H3K27me3_rep1	ChIP-seq
GSM4914879	tor-es_H3K27me3_rep2	ChIP-seq
GSM4914880	tor-es_H3K27me3_rep3	ChIP-seq
GSM4914881	Col-0_H3K9me2_rep1	ChIP-seq
GSM4914882	Col-0_H3K9me2_rep2	ChIP-seq
GSM4914883	Col-0_H3K9me2_rep3	ChIP-seq
GSM4914884	tor-es_H3K9me2_rep1	ChIP-seq
GSM4914885	tor-es_H3K9me2_rep2	ChIP-seq
GSM4914886	tor-es_H3K9me2_rep3	ChIP-seq
GSM5772261	DMSO_H3K27me3_rep1	ChIP-seq
GSM5772262	DMSO_H3K27me3_rep2	ChIP-seq
GSM5772263	DMSO_H3K27me3_rep3	ChIP-seq
GSM5772264	AZD8055_H3K27me3_rep1	ChIP-seq
GSM5772265	AZD8055_H3K27me3_rep2	ChIP-seq
GSM5772266	AZD8055_H3K27me3_rep3	ChIP-seq
GSM5772267	Torin2_H3K27me3_rep1	ChIP-seq
GSM5772268	Torin2_H3K27me3_rep2	ChIP-seq
GSM5772269	Torin2_H3K27me3_rep3	ChIP-seq

Genome browser session
(e.g. [UCSC](#))

http://bioinfo.sibs.ac.cn/TOR_PRC2

Methodology

Replicates	Three biological replicates.
Sequencing depth	Approximately 15-20 million paired-end reads per sample with 100-150bp total read length.
Antibodies	Mouse anti-Histone H3K9me2 antibody (Abcam, Cat# ab1220, 1:200) and Rabbit anti-Histone H3K27me3 Antibody (Sigma-Aldrich, Cat# 07-449, 1:200) were used for ChIP-Seq.
Peak calling parameters	The ChIP-seq reads were mapped to Arabidopsis (TAIR10) and human (hg19) combined genomes, using BWA-MEM (version 0.7.15-r1142-dirty). MACS2 utility callpeak was used to identify read-enriched regions (peaks) and utility pileup was used to generate bedgraph files with default settings. The number of reads in the bedgraphs was then scaled by the reference derived normalization factor to generate reference-adjusted reads per million (RRPM).
Data quality	The quality of each sequencing library was assessed by examining fastq files with FastQC (version 0.11.5).
Software	Trimmomatic (version 0.36). BWA-MEM (version 0.7.15-r1142-dirty). Samtools (version 1.6) MACS2 BedGraphToBigWig (version 4) JBrowse (version 1.12.1)